Reanalysis of NOAA H_2 observations: implications for the H_2 budget

Fabien Paulot[1], Gabrielle Pétron[2,3], Andrew M. Crotwell[2,3], and Matteo B. Bertagni[4,5]

[1]Geophysical Fluid Dynamics Laboratory, National Oceanic and Atmospheric Administration, Princeton, NJ, USA
[2]Cooperative Institute for Research in Environmental Sciences, University of Colorado Boulder, Boulder, CO, USA
[3]Global Monitoring Laboratory, National Oceanic and Atmospheric Administration, Boulder, CO, USA
[4]High Meadow Environmental Institute, Princeton University, Princeton, NJ, USA
[5]Department of Civil and Environmental Engineering, Princeton University, Princeton, NJ, USA

Correspondence: Fabien Paulot (fabien.paulot@noaa.gov)

Abstract. Hydrogen (H_2) is ~~being considered for many applications as an~~ a promising low-carbon alternative to fossil fuels ~~. Robust assessment of the climate implications of increased~~ for many applications. However, significant gaps in our understanding of the atmospheric H_2 budget limit our ability to predict the impacts of greater H_2 usage~~in the global economy is partly hindered by uncertainties in its biogeochemical cycle~~. Here we use NOAA H_2 dry air mole fraction observations from air samples collected from ground-based and ship platforms from 2010 to 2019 to evaluate the representation of H_2 in the NOAA GFDL-AM4.1 atmospheric chemistry-climate model. We find that the ~~model~~ base model configuration captures the observed interhemispheric gradient well but underestimates the surface concentration of H_2 by about 10 ~~ppbv. Observations show a~~ ppb. Additionally, the model fails to reproduce the 1-2 ~~ppbv~~ppb/year mean increase in surface H_2 observed at background stations~~, while the simulated H_2 exhibits no significant change over the 2010–2019 period~~. We show that ~~this model bias is primarily driven by the estimated decrease of~~ the cause is likely an underestimation of current anthropogenic emissions, ~~mostly from transportation, and that including leakage from H_2~~including potential leakages from H_2-producing facilities~~can improve the simulated trend. We find~~. We also show that changes in soil moisture, soil temperature, and snow cover ~~likely increase the magnitude and modify the spatial distribution~~ have likely caused an increase in the magnitude of the soil sink, the most important removal mechanism for atmospheric H_2, especially in the Northern Hemisphere. However, ~~the magnitude and even the sign of such changes is uncertain~~ there remains uncertainty due to fundamental gaps in our understanding of ~~H_2~~ H_2 soil removal, such as the minimum ~~soil moisture for H_2 soil uptake. We~~ moisture required for H_2 soil uptake, for which we performed extensive sensitivity analyses. Finally, we show that the observed meridional gradient of the H_2 mixing ratio and its seasonality can provide important constraints to test and refine parameterizations of the H_2 soil ~~removal~~sink.

1 Introduction

Increased hydrogen (H_2) usage has been proposed as a strategy to reduce the carbon intensity of many sectors of the economy that are difficult to electrify (Hydrogen Council, 2017; da Silva Veras et al., 2017; Staffell et al., 2019; Abe et al., 2019; Dawood et al., 2020). The climate benefits of greater ~~hydrogen~~ H_2 usage depend primarily on the H_2 production pathway.

Current ~~hydrogen~~ H_2 production is dominated by steam reforming of methane (CH_4) in natural gas (Holladay et al., 2009; International Energy Agency, 2019), a process that is very carbon intensive (Howarth and Jacobson, 2021). Carbon capture can reduce CO_2 emissions associated with ~~hydrogen productionbut the increased demand for CH_4 may~~ H_2 production. However, methane leakage throughout the supply chain could offset much of the expected climate benefits of increased H_2 usage (Howarth and Jacobson, 2021; Ocko and Hamburg, 2022; Bertagni et al., 2022; Hauglustaine et al., 2022). Alternative production pathways such as renewable-based electrolytic H_2 ~~have been estimated to~~ can provide large and rapid reductions in radiative forcing (Hauglustaine et al., 2022), and considerable investments have been devoted to reducing their cost (International Energy Agency, 2022). Furthermore, evidence of ~~high~~ significant concentrations of H_2 in ~~many different geologic environments (Zgonnik, 2020)~~ surface and subsurface natural gases (Zgonnik, 2020; Milkov, 2022; Lefeuvre et al., 2021) have spurred interest in the potential of ~~naturally-occurring~~ naturally occurring H_2 as a new primary energy source (Prinzhofer et al., 2018; Lapi et al., 2022).

H_2 photooxidation in the atmosphere also tends to increase CH_4, O_3, and stratospheric water vapor, which results in indirect radiative forcing (Derwent et al., 2001; Paulot et al., 2021). Sand et al. (2023) recently calculated that H_2 has a global warming potential of $\simeq 11.6 \pm 2.8$ and 37.3 ± 15.1 for a 100 and 20-year time horizon, respectively.

~~Assessing the potential climate benefits of greater~~ Significant uncertainties regarding the overall budget of H_2 ~~usage also requires us to quantify the environmental impact of~~ remain. H_2 sources include both emissions and photochemical production from the oxidation of volatile organic compounds (VOCs). Estimates for the overall source of atmospheric H_2 range from $\simeq$ 70 to 110 Tg/yr, a large spread primarily associated with the magnitude of the ~~atmospheric release of~~ H_2 ~~. Recent studies indicate that~~ photochemical sources (Ehhalt and Rohrer, 2009). Recent work also argues that current estimates of H_2 ~~has a global warming potential (100 years) of $\simeq$ 10 (Derwent, 2022; Warwick et al., 2022; Hauglustaine et al., 2022). The radiative impact~~ sources need to be revised upward to account for geologic H_2 seepage (Zgonnik, 2020). These uncertainties in the nature and magnitude of H_2 ~~is indirect, reflecting the increase in CH_4, O_3, and stratospheric water vapor associated with its photooxidation (Derwent et al., 2001; Paulot et al., 2021).~~ sources have proved challenging to reduce in part because of commensurate uncertainties in H_2 ~~photooxidation is~~ sinks. The atmospheric oxidation of H_2 by OH is well understood but is estimated to account for ~~20-30%~~ less than one third of the overall ~~sink~~ atmospheric sink (Ehhalt and Rohrer, 2009; Paulot et al., 2021) . The most important removal pathway is the consumption of H_2 ~~, which is dominated by soil uptake (Ehhalt and Rohrer, 2009). As a result, the soil sink tends to reduce the indirect radiative forcing~~ by high-affinity hydrogen oxidizing bacteria (HA-HOB), a class of bacteria that have been identified in many different soils (Constant et al., 2008; Greening et al., 2015; Bay et al., 2021; Greening an . Several parameterizations of the H_2 soil sink have been developed (Ehhalt and Rohrer, 2013; Price et al., 2007; Smith-Downey et al., 2006 that aim at capturing the observed sensitivity of H_2 ~~.~~ soil removal to soil temperature, soil moisture and ecosystem/soil type (Ehhalt and Rohrer, 2009). However, observational constraints on H_2 soil removal remain very limited (Meredith et al., 2016) and this process remains challenging to represent in global models (Yashiro et al., 2011; Paulot et al., 2021).

~~We recently presented an assessment of H_2 indirect radiative forcing using the Geophysical Dynamics Laboratory (GFDL) AM4.1 model (Paulot et al., 2021).~~ Here, we leverage the recently completed recalibration of H_2 measurements collected by NOAA Global Monitoring Laboratory ~~. This~~ to perform a comprehensive evaluation of the simulation of H_2 in the Geophysical

Dynamics Laboratory (GFDL) AM4.1 model (Horowitz et al., 2020; Paulot et al., 2021). The NOAA monitoring network provides additional spatial coverage that complements other existing networks (AGAGE (Prinn et al., 2018), CSIRO (Francey et al., 2003)) . Here, and offers a unique opportunity to evaluate the skill of the model in capturing changes in H_2 atmospheric concentration since 2010. This period is especially important to gain a quantitative understanding of the present-day H_2 budget, also given that recent H_2 observations at Mace Head (Derwent et al., 2021, 2023) show both an increase in H_2 concentration and its soil removal rate. The study is organized as follows: we first describe and evaluate the representation of H_2 in the GFDL-AM4.1 global chemistry-climate model, focusing on changes in H_2 over the 2010–2019 period. We then evaluate the impact of assess the sensitivity of the H_2 anthropogenic sources and soil removal on the simulated seasonality and trends of simulations to uncertainties in the H_2 budget focusing on the representation of anthropogenic H_2 emissions and soil removal.

2 Methods

2.1 Observations

NOAA Global Monitoring Laboratory (GML) provides long-term monitoring of long-lived greenhouse gases and other trace species. The NOAA GML Global Cooperative Air Sampling Network is a partnership between GML and many outside organizations and individual volunteers to collect discrete air samples approximately weekly from 60+ globally distributed sites (Global Monitoring Laboratory, 2023). These sites are often situated to collect air representative of large regional air masses. Priorities are placed on sites where opportunities exist for local support which can be maintained over long (decadal) time scales. The discrete air samples are collected weekly in pairs of 2 L glass flasks and are returned to GML for measurements of multiple species on central measurement systems thus providing a high level of consistency across the globally distributed network. (add references)

GML measurements of H_2 in the discrete air samples began in the late 1980's as an opportunistic measurement associated with the analytical technique then used for measuring atmospheric carbon monoxide (CO). To facilitate these H_2 measurements, NOAA/GML developed an in-house H_2-in-air reference scale based on a few gravimetric standards (the latest iteration named H2-X1996). This reference scale was not stable over time and introduced significant time-dependent measurement errors. GML recently converted part of the historical H_2 measurement records to the H_2 calibration scale recommended by the World Meteorological Organization (WMO/MPI H2-X2009) maintained by Max Planck Institute (MPI) in Jena, Germany (Jordan and Steinberg, 2011). Measurements since approximately 2010 have been reprocessed onto the MPI scale to remove the biases inherent in the NOAA X1996 scale . (Pétron et al, in preparation). NOAA reprocessed H_2 (Pétron et al., submitted). NOAA reprocessed H_2 data since 2010 is consistent with other measurement labs which maintain tight connections to the MPI central calibration facility to within 1-2 ppbv on an annual basis for same air measurements with CSIRO and the MPI-BGC (Pétron et al., submitted). However, earlier NOAA data that remains on the obsolete NOAA X1996 scale is known to be biased relative to the later NOAA data and to other monitoring programs.

Here, we only consider ground stations from the NOAA cooperative air sampling network with at least 96 distinct monthly observations over the 2010-2019 period (80% coverage, Fig. S1). Ship-based observations are binned in 4°x4° regions and we only consider regions with at least 40 observations.

2.2 ~~Global model~~Model setup

We use the GFDL Atmospheric Chemistry Model AM4.1 (Horowitz et al., 2020). For all configurations, the model is run from 2004 to 2019. Monthly sea surface temperature and sea ice concentration are from Rayner et al. (2003) and Taylor et al. (2000). Horizontal winds are nudged to 6-hourly horizontal winds from the National Center for Environmental Prediction (Kalnay et al., 1996) . The model output is sampled at the time and location of the air sampling. To better quantify the drivers of the H_2 distribution and trend, we tag H_2 associated with anthropogenic, marine, soil, and biomass burning direct H_2 emissions and H_2 produced by the oxidation of VOCs.

2.2.1 BASE simulation

AM4.1 includes a detailed representation of H_2 (Paulot et al., 2021), which is briefly summarized here. This configuration will ~~hereafter~~ be referred to as BASE (Table 1), hereafter. H_2 sources include both direct ~~emissions and photochemical productions~~emission from anthropogenic and natural sources as well as photochemical production. Anthropogenic emissions of H_2 ($\simeq$ 13 Tg/yr over the 2010–2019 period) are estimated from CO emissions in the Community Emissions Data System (CEDS) v20210421 (O'Rourke et al., 2021) using time-invariant sector–specific emission H_2:CO emissions ratios (Table ~~??).~~ S1). The transportation and residential sectors are the largest contributors to anthropogenic H_2 emissions (Fig. S2). Biomass burning emissions ($\simeq$ 8 Tg/yr) are estimated using the Global Fire Emissions Database (GFED4s, van der Werf et al. (2017)) with emission factors from Akagi et al. (2011) and Andreae (2019). Marine (6 Tg/yr) and terrestrial (3 Tg/yr) sources of H_2 are prescribed as a monthly climatology ~~based on Paulot et al. (2021).~~ and distributed spatially (Fig. S3) based on the soil and marine CO emission patterns in the Precursors of Ozone and their Effects in the Troposphere inventory (Granier et al., 2005). The BASE emission inventory does not include geological sources of H_2.

The production of H_2 ~~is also produced from the photolysis of formaldehyde (~~associated with CH_2O ~~)~~photolysis is calculated interactively using FAST-JX version 7.1, as described by Li et al. (2016). Formaldehyde sources are dominated by the oxidation of ~~volatile organic compounds (VOCs)~~ VOCs from anthropogenic (O'Rourke et al., 2021), biomass burning (van der Werf et al., 2017), and natural origins. Biogenic emissions of VOCs are prescribed as a monthly climatology (Granier et al., 2005), except for isoprene and terpenes, of which emissions are calculated interactively using the Model of Emissions of Gases and Aerosols from Nature (Guenther et al., 2012). Surface CH_4 is prescribed as a monthly latitudinal profile from observations up to 2014 (Meinshausen et al., 2017) and from the SSP1-2.6 scenario after 2015 (Meinshausen et al., 2020). We select this scenario as it tracks well the observed global CH_4 surface mixing ratio from the World Meteorological Organization Global Atmospheric Watch greenhouse gases observational network (WMO, 2021). To characterize the contribution of different VOC emissions to the photochemical production of H_2, we perform a set of sensitivity experiments in which we perturb the emission of a given VOC by 10% and quantify the response of H_2 production. For CH_4 oxidation, we directly track the different oxidation pathways that result in H_2 production. The molar yield of H_2 from CH_4, isoprene, methanol, and terpene are estimated to be 0.38, 0.57, 0.21, and 0.66 mol/mol, respectively. These yields are broadly similar to estimates derived by Ehhalt and Rohrer (2009) (0.37, 0.54, 0.19, 0.71, respectively) but are lower than estimates derived from box-model (0.38, 0.83, 0.38, and 0.85, respectively for NO_x=160 pptv (Grant et al., 2010)), which may reflect the impact of wet and dry deposition. In particular, Fig. S4 shows that the simulated yield of H_2 from CH_4 oxidation is lowest in the tropics, where most CH_4 is oxidized, as a greater fraction of CH_2O is oxidized by OH in this region than at high latitudes.

Global source of H_2 (black, panel a). Dotted wedges indicate photochemical sources. Panel b shows the changes in the magnitude of H_2 sources over the 2010–2019 period. For clarity, the green line denotes the combined change in H_2 emissions and photochemical production from natural sources (marine and soil emissions + BVOCs photooxidation). Overall, we find that CH_4 oxidation is the largest photochemical source of H_2 ($\simeq$27 Tg/yr). The oxidation of biogenic VOCs (BVOCs) accounts for the majority of the remaining photochemical source of H_2 ($\simeq$ 14 Tg/yr) primarily from isoprene (8 Tg/yr), methanol (3 Tg/yr), and terpene (1 Tg/yr). The oxidation of VOCs from anthropogenic and biomass burning origin produces $\simeq$3 Tg/yr of H_2. Our estimates are in good agreement with previous estimates (Ehhalt and Rohrer, 2009): CH_4 (23 $\pm$ 8 Tg/yr), isoprene (9 $\pm$ 6 Tg/yr), biomass burning and anthropogenic VOCs (3 Tg/yr). This similarity can attributed to the similar yield of H_2 from CH_2O (0.4 mol/mol compared to 0.37 (Ehhalt and Rohrer, 2009)). More work is needed to better characterize the temperature and pressure sensitivity of CH_2O photolysis quantum yields (Röth and Ehhalt, 2015).

Fig. 1a summarizes the simulated sources of H_2 associated with photochemical production and direct emissions in the BASE run. Over the 2010-2019 period, the average global simulated source of H_2 is 74$\pm$1 Tg/yr, with 60% from photochemical production. Anthropogenic activities are estimated to account for $\simeq$ 40% of the overall H_2, primarily from the CH_4 oxidation. Note that we assume that 50% of the photochemical production of H_2 from CH_4 oxidation is anthropogenic based on the detailed bottom-up inventory of CH_4 sources (Saunois et al., 2020). Top-down estimates suggest a higher contribution of anthropogenic sources ($\simeq$ 60%, Saunois et al. (2020)), which would further increase the fraction of H_2 associated with anthropogenic activities. Fig. 1b shows that the simulated total source of H_2 changes little over the 2010–2019 period. The simulated annual photochemical source of H_2 is 1.6 Tg/yr greater in 2017-2019 than in 2010-2012, with 70% of this increase attributed to CH_4. In contrast, H_2 associated with anthropogenic activities decreases (-1.3 Tg/yr, Fig. S2a), mostly from transport (-1 Tg/yr) and industries (-0.4 Tg/yr). The decrease in H_2 emissions reflects the decline in CO emissions from these sectors. The interannual variability of the overall H_2 source over the 2010-2019 period is dominated by the variability of biomass burning emissions, which can result in interannual changes of $\simeq$ 2 Tg/yr.

H_2 sinks include chemical oxidation by OH and O(^{1}D), and soil uptake associated with microbial activity. In the BASE configuration, the The deposition velocity of H_2 ($v_d(H_2)$) over land is calculated following the parameterization of Ehhalt and Rohrer (2013) and depends on temperature, soil moisture (Ehhalt and Rohrer, 2013) and soil carbon (Khdhiri et al., 2015; Paulot et al., 2021). Here, we drive the BASE simulation with In the BASE configuration we use a monthly climatology of $v_d(H_2)$ calculated using monthly meteorological and soil outputs from the GFDL Earth System Model ESM4.1 over the 1989–2014 period (Dunne et al., 2020; Paulot et al., 2021). Soil uptake is estimated to account for 71% of the overall H_2 sink. The

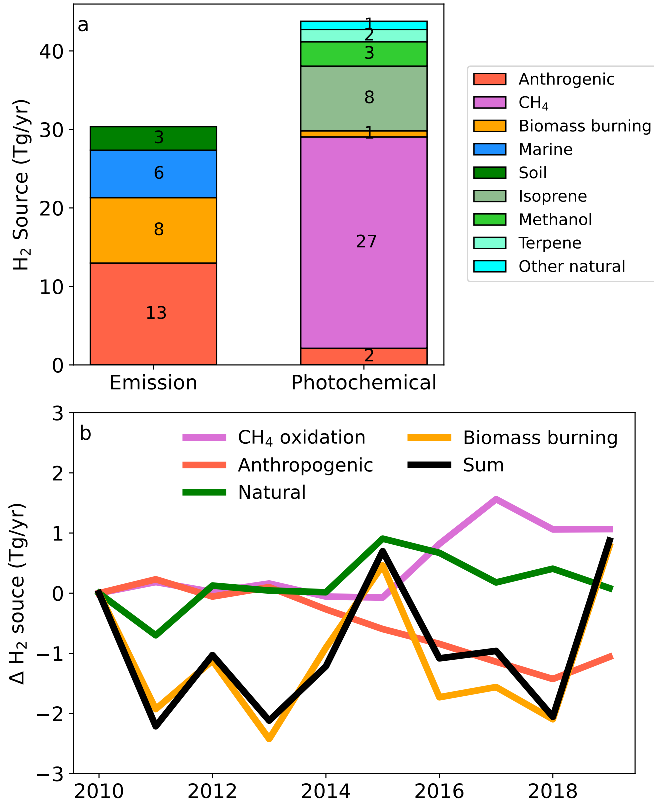

Figure 1. Global source of H_2 (panel a). Panel b shows the changes in the magnitude of H_2 sources over the 2010–2019 period. For clarity, the green line denotes the combined change in H_2 emissions and photochemical production from natural sources (marine and soil emissions + BVOCs photooxidation).

overall lifetime of H_2 in the BASE configuration is 2.5 years. The lifetime of H_2 associated with anthropogenic emissions is 6% shorter due to their geographical distribution.

In addition to the BASE configuration, we perform sensitivity simulations using an expanded treatment of

2.2.2 Sensitivity simulations

In this section, we describe additional model simulations that are designed to explore the impact of uncertainties in the representation of H_2 emissions (REVISED) and emission and deposition on the simulation of atmospheric H_2 soil removal (REVISED_GLDAS, REVISED_GLDAS2). All model configurations are summarized in Table 1(Table 1). We focus on H_2 emissions and deposition as their representations in models are largely derived from limited observational constraints (Derwent et al., 2023; Paulot et al., 2021).

The REVISED emission inventory is described in Appendix . Focusing on anthropogenic emissions, it includes a more revised configuration focuses on the representation of anthropogenic and natural H_2 to CO emission ratios based on , including a more compehensive treatment of emissionsfrom the transportation sectors based on measurements by emissions. The development of the REVISED emission inventory is guided by the biases of the BASE configuration against H_2 observations (Supporting materials S1.1, Ghosh et al. (2015)).

In the BASE simulation, $\simeq$ 80% of In particular, we focus on the representation of transportation emissions (Table S1) and emissions associated with industrial H_2 emission originate from the transportation and residential sectors (Fig. ??a). Global anthropogenic emissions are 1.4 Tg/yr lower in 2019 compared to 2010, with the largest decline from the transportation (-1 Tg/yr)and industrial (-0.4 Tg/yr) sectors, respectively. Fig. ??b shows a revised anthropogenic inventory for H_2, which is described in Appendix ??.

In the REVISED emission inventory, we incorporate a more detailed treatment of transportation and industrial emissions . In particular, we include H_2 leakage from industrial production of H_2 use for refining, ammonia, methanol and steel production, assuming a time-invariant leakage rate of 2%, consistent with recent estimates (2.7% (Fan et al., 2022), 1.2% (Arrigoni and Bravo Diaz, 202). We estimate that the increase in H_2 demand from these sectors (+$\simeq$ 18 Tg/yr in 2019 relative to 2010 (International Energy Agency, 2019)) has resulted in $\simeq$0.3 Tg/yr more H_2 emissions over the 2010-2019 period. The REVISED anthropogenic emissions are estimated to be 14.1 Tg/yr in 2010 and 13.5 Tg/yr in 2019, a lower decrease than in the BASE configuration, which is consistent with the missing emissions inferred from equation ??. However, . Further details regarding the treatment of anthropogenic and natural sources in the updated treatment of anthropogenic emissions does not explain the low bias in the simulated REVISED emission inventory can be found in the Supporting materials (Texts S1.2 and S1.3)

We further consider the impact of a different representation of H_2 mixing ratio. Ehhalt and Rohrer (2009) surveyed many "minor" sources of H_2, soil uptake on the simulation of H_2. Here, we use the parameterization of the combined magnitude of which could amount to 2 Tg/yr. For instance, we do not include geological sources of H_2, the magnitude of which carries considerable uncertainty (0-30 Tg/yr (Zgonnik, 2020)). In the REVISEDsimulation, we increase the H_2 soil source from 3 Tg/yr to 4.5 Tg/yr as described in Appendix ??. Clearly more observational constraints are needed to develop a more robust soil moisture response of HA-HOB activity recently developed by Bertagni et al. (2021). This parameterization relates the minimum soil moisture required for H_2 emission inventory.

The model is run from 2004 to 2019. Monthly sea surface temperature and sea ice concentration are from Rayner et al. (2003) and Taylor et al. (2000). Horizontal winds are nudged to 6-hourly horizontal winds from the National Center for Environmental Prediction (Kalnay et al., 1996). The model output is sampled at the time and location of the air sampling. To better quantify the drivers of the uptake by HA-HOB to soil hydrological properties, which facilitates its incorporation in global models. This model also allows to vary the strength of the diffusion barrier associated with soil litter, which can reduce H_2 distribution and trend, we add five different tracers that represent transport to active sites (Smith-Downey et al., 2008; Ehhalt and Rohrer, 2009) . To quantify possible changes in v_d(H_2associated with anthropogenic, marine, soil, and biomass burning direct) over the 2010-2019 period, we calculate daily deposition velocity using 3-hourly soil moisture, soil temperature, and snow cover from the NASA Global Land Data Assimilation System (Rodell et al., 2004). We focus on two different configurations. In REVISED_GLDAS, we neglect the litter resistance and assume that HA-HOB activity is inhibited when the soil matrix potential (Ψ_{ws}) is less than the wilting point of plants in semiarid environments ($\Psi_{ws} = -3000$ kPa) as recommended by

Table 1. Model configurations

	H_2 anthropogenic emission	H_2 natural emission
BASE	Time-invariant ~~emissions factor~~ H_2:CO ~~(Paulot et al., 2021)~~ emission ratio (Table S1)	Ocean+Soil: Monthly climatology Biomass burning: ~~GFED~~ GFED4s
REVISED	~~Time-varying emissions factor~~ Revised H_2:CO emission ratio ~~Appendix ??~~ Emission from industrial H_2 use (Text S1.2 and Table S1)	Ocean: Calculated from CO seawater ~~distribution~~ concentration Soil: Calculated from ~~biological nitrification~~ N fixation ~~Appendix ??~~ (Text S1.3) Biomass burning: same as BASE
REVISED_GLDAS	same as REVISED	Same as REVISED
REVISED_GLDAS2 ~~Appendix ??~~	same as REVISED	Same as REVISED

Bertagni et al. (2021). The required soil moisture for the H_2 ~~emissions and H_2 produced by VOC oxidation~~uptake is not well known and experimental studies have shown that HA-HOB are present in very arid environments (Jordaan et al., 2020). In REVISED_GLDAS2, we assume a much lower activation threshold for HA-HOB ($\Psi_{ws} = -10,000$ kPa) and account for the litter barrier. Note that both these configurations use the REVISED emission inventory. More details regarding the calculation of $v_d(H_2)$ can be found in the Supporting materials (Text S1.4).

3 Results and discussion

3.1 ~~Global budget~~BASE model evaluation

~~Fig. 1a summarizes the simulated sources of H_2 associated with photochemical production (dots) and emissions (solid color). Over the 2010-2019 period, the average global simulated source of H_2 is 74.1±1 Tg/yr. The contribution of CH_4 oxidation is estimated by separately tracking the different CH_4 oxidation pathways that result in H_2 production. The contribution of other photochemical pathways is estimated by perturbing the associated precursor emissions by 10%.~~

3.1.1 Climatology

CH_4 oxidation is the single largest source of H_2 (29.6 Tg/yr) accounting for $\simeq 40\%$ of the overall H_2 source and 2/3 of its photochemical source. This contribution is larger than estimated by Ehhalt and Rohrer (2009) (23 Tg/yr, 30% and 56% in 2005, respectively). Two factors contribute to this difference: a) greater oxidative flux of CH_4 (560 Tg/yr, $+\simeq 12\%$) and b) higher yield of H_2 from CH_4 oxidation (0.42 mol(H_2)/mol(CH_4) compared to 0.37 mol(H_2)/mol(CH_4)).

The second most important photochemical source of H_2 is the photooxidation of isoprene. Isoprene is primarily emitted from plant foliage and accounts for $\simeq 50\%$ of the global emissions of non-methane volatile organic carbon (NMVOC, Guenther et al. (2006)). We estimate that the oxidation of isoprene yields $\simeq 0.1$ mol(H_2)/mol(C), similar to (Ehhalt and Rohrer, 2009), which amounts to $\simeq 6.9$ Tg/yr or $\simeq 9\%$ of the overall source of H_2). The oxidation of other biogenic NMVOCs accounts for the majority of the remaining photochemical source of H_2 ($\simeq 4.9$ Tg/yr) with smaller contributions from the photooxidation of NMVOCS from anthropogenic (2.3%) and biomass burning (0.9%) origin. Anthropogenic activities are estimated to contribute over 40% of the overall H_2 source including 17.5% from direct emissions (associated with fossil fuel combustion), 2.3% from NMVOC oxidation, and 22% from CH_4. The CH_4 estimate is obtained by scaling the global source of H_2 from CH_4 by the estimated contribution of anthropogenic sources to CH_4 emissions (50-62% (Saunois et al., 2020)).

The simulated total source of H_2 changes little over the 2010–2019 period. The annual production of H_2 associated with the photooxidation of CH_4 and NMVOCs is 1.25 Tg/yr and 1.45 Tg/yr (0.95 Tg/yr from isoprene) greater in 2019 than in 2010, respectively. This increase is largely compensated by a decrease in emissions of H_2 associated with anthropogenic activities (-1.93 Tg/yr). As we will discuss in section 3.1.1, this decline is primarily driven by a decrease in anthropogenic CO emissions from the transportation sector and assuming the same behaviour for H_2 emissions. The interannual variability of the overall H_2 source over the 2010-2019 period is dominated by the variability of biomass burning emissions.

The overall lifetime of H_2 in the BASE configuration is 2.5 years. The lifetime of H_2 associated with anthropogenic emissions is 6% shorter due to their geographical distribution. Soil uptake is estimated to account for 71% of the overall H_2 sink.

3.2 Evaluation

Fig. 2 shows the average model bias against surface observations from NOAA GML. In the BASE configuration, AM4.1 underestimates H_2 at all stations, with greater biases over continental regions (Fig. 2). Correlations exceed 0.5 at more than 90% of background sites (square) but only at 55% of continental sites. Fig. 2b further shows that the magnitude of the pole to pole gradient (concentration at the South pole is $\simeq 50$ ppbv) ppb greater than at the North pole, which is well captured . by the BASE configuration.

To examine differences between the model and observed seasonality, we first apply the Kmean++ clustering algorithm (Arthur and Vassilvitskii, 2007) to the observed H_2 monthly climatology. Since our focus is on the seasonality of H_2 we transform the monthly climatology of H_2 at each site such that it has a mean of 0 and a standard deviation of 1. Using the within-cluster sum of squares and the silhouette score, we find that the standardized H_2 observations can be well represented using 4 clusters. Fig. 3 shows the seasonality of the standardized H_2 concentration for each cluster (panel a) as well as their spatial distribution (panel b). Sites are found to cluster broadly by latitude based on the seasonality of H_2 with clusters 1, 2, 3,

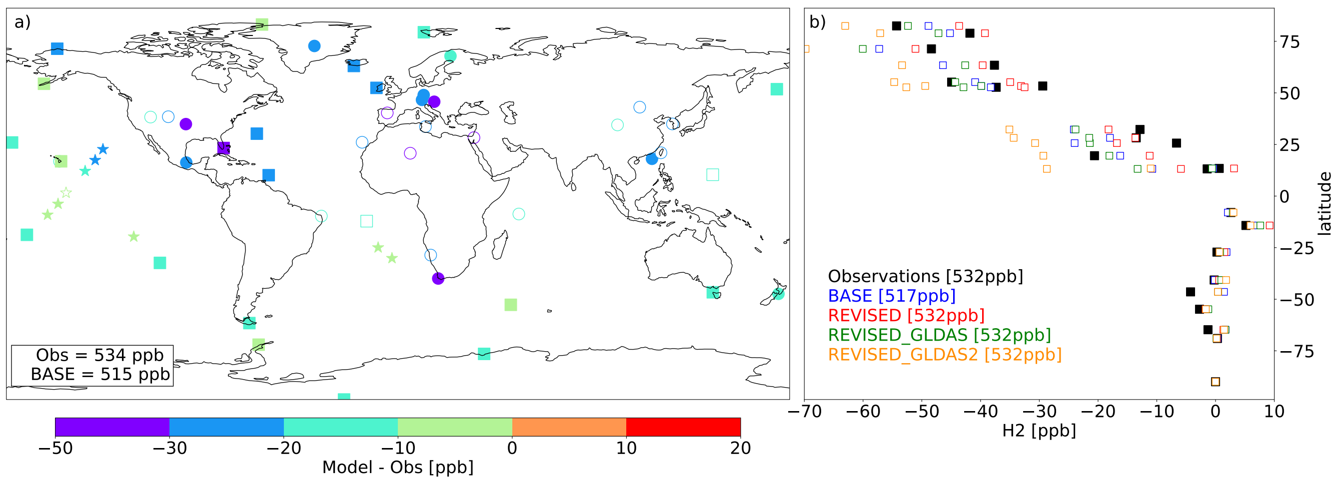

Figure 2. Mean model bias at individual sites for the BASE model configuration (a) over the ~~2009–2019~~ 2010–2019 period. Filled symbols denote sites where the correlation between observed and simulated H_2 concentrations exceeds 0.5. Square and star symbols denote background sites and cruises, respectively. Panel (b) shows the observed and simulated difference in H_2 at background sites relative to H_2 mole fraction measured at the South Pole observatory. The average concentrations at background sites is indicated for each configuration in the legend.

and 4 being comprised primarily of sites located in the Southern mid to high latitudes, Southern tropics, Northern subtropics, and Northern mid to high latitudes, respectively. The model captures the seasonality of H_2 well in the Southern Hemisphere (cluster 1) but peaks 1 to 3 months earlier than observations for clusters 2, 3 and 4. Fig. 3c shows the contribution of different sources of H_2 to the simulated seasonality of H_2 (inferred from the tagged H_2 tracers). The seasonal bias for cluster 2 is primarily driven by H_2 emitted from biomass burning, which peaks $\sim$ 2 months earlier than observations. This delay may be associated with greater burning of woody material towards the end of the dry season, emitting more incompletely oxidized products such as H_2 (van der Werf et al., 2006). Fig. 3c also shows that the seasonal bias in clusters 3 and 4 may be associated with H_2 emitted by anthropogenic activities. As we will show in section 3.1.1, this seasonal bias may also reflect errors in the removal of H_2.

3.1.1 Time series

Fig. 4 shows ~~*that*H_2~~ that H_2 has increased at most sites with an average trend at background sites of 1.4±0.7 ~~ppbv~~ppb/yr over the 2010-2019 period with little variability with latitude. Trends are calculated using ~~ordinary-least-square~~ ordinary least-square regression applied to the deseasonalized monthly H_2 concentrations. In contrast, ~~no significant change in~~ simulated H_2 concentration ~~is simulated~~ in the BASE configuration ~~(0.045±0.4 ppbv/yr at background sites)~~changes little over this time period.

In the Northern hemisphere, the lack of trend at background sites in the ~~simulated H_2 concentration~~ model (Fig. 4c) reflects the ~~cancellation~~ near-cancellation between the increase of photochemically-produced H_2 and the decrease of H_2 emitted from

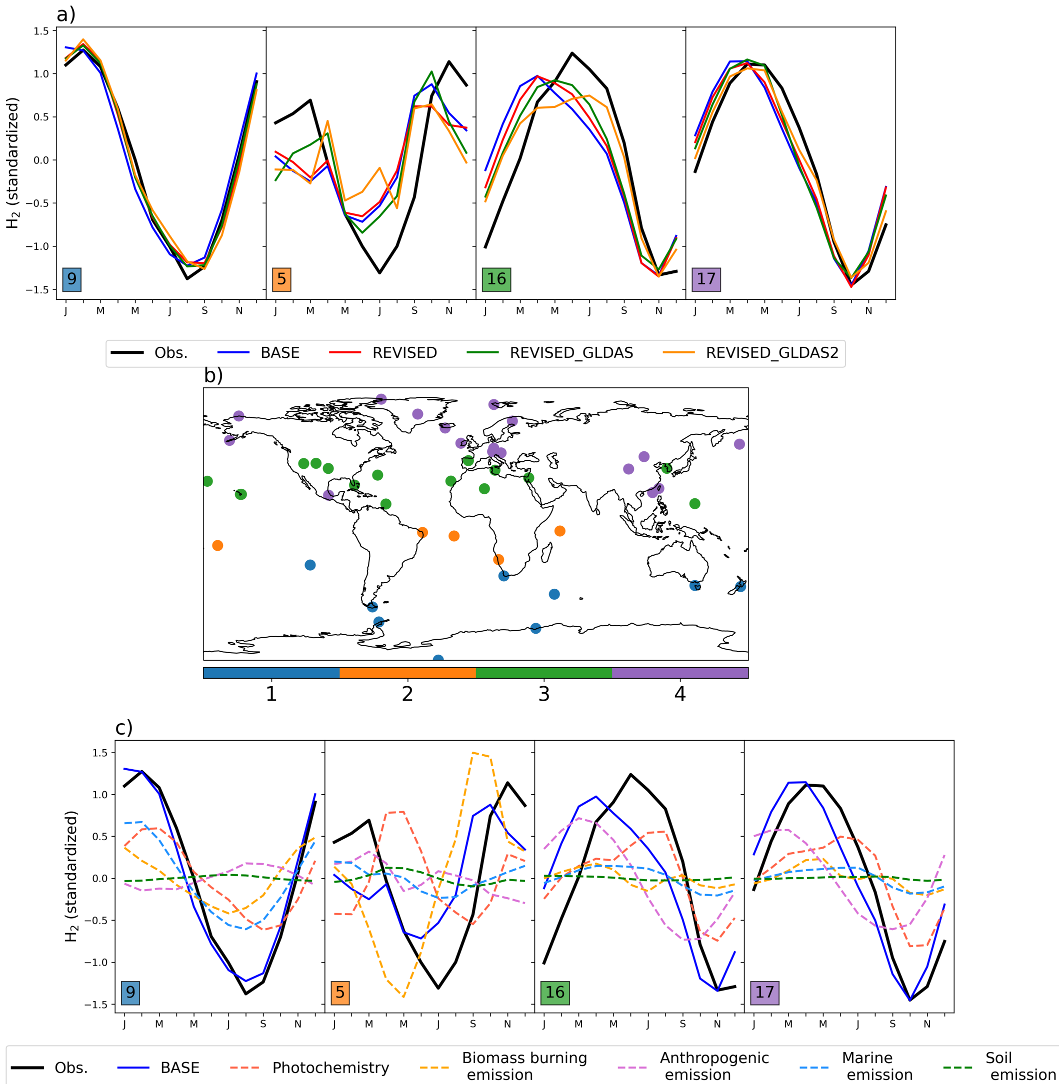

Figure 3. Monthly standardized H_2 concentration for each cluster (a). The number of sites in each cluster is indicated by insets. The sites included in each cluster are shown in panel (b). The variation of source-tagged H_2 tracers in each cluster is shown in panel (c). Source-tagged H_2 tracers are normalized using the standard deviation of simulated H_2.

anthropogenic sources. , consistent with the changes in anthropogenic emissions and the photochemical source of H_2 from CH_4 and biogenic VOCs oxidation (Fig. 1). The simulated absolute trend in anthropogenic hydrogen is $\simeq 50\%$ lower in the Southern Hemisphere relative to the Northern Hemisphere due to the higher relative areal density of anthropogenic sources in the Northern Hemisphere. In contrast, the change in photochemically-produced H_2 exhibits little variability with latitude and matches the observed trend well. The simulated trend also shows little latitudinal variation due to a decrease in H_2 from biomass burning in the Southern Hemisphere.

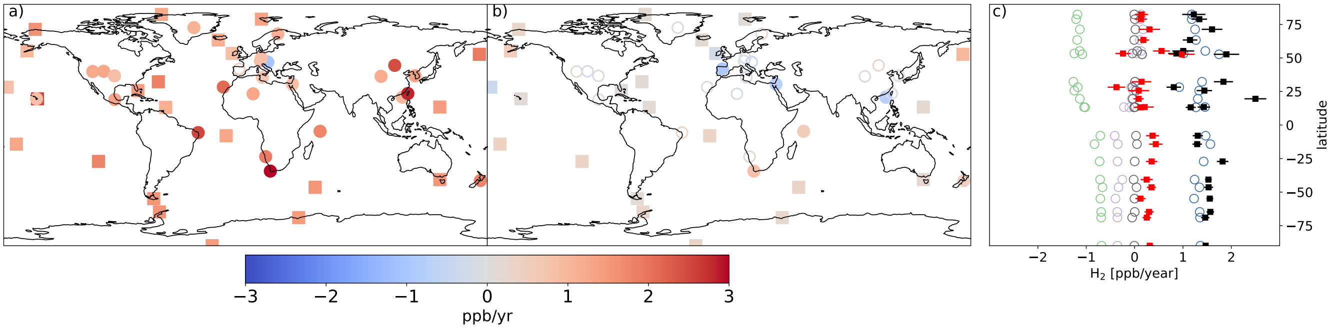

Figure 4. Trend in H_2 concentrations in observations (a) and in the BASE simulation (b) over the 2010–2019 period. Panel (c) shows the observed (black) and simulated (red) trend in H_2 at background sites (squares) as well as the trend in tagged H_2 tracers associated with anthropogenic sources (green), biomass burning (purple), ocean+soil sources (black), and photochemical production (blue). Filled symbols denote trends that are significantly different from 0 (p<0.01). The error bars show one standard deviation for the estimated observed and simulated trends.

4 ~~Discussion~~

3.1 Sensitivity simulations

~~The BASE simulation was tuned against seasonal mean ground-based~~ In this section, we explore how uncertainties in the representation of H_2 ~~mole fraction reported by NOAA, CSIRO and AGAGE over the 1995-2005 period (Paulot et al., 2021). As detailed in Pétron et al (in preparation), the X1996 calibration scale used for NOAA observations for the 1995-2005 period induced not only a bias but also a drift in NOAA H_2 observations. The model evaluation against the more recent and recalibrated NOAA dataset highlights significant~~ emissions and deposition contribute to the biases in the ~~simulated mean concentration, trend, and seasonality of H_2 in the BASE configuration (section 3). Here, we evaluate the constraints that the recalibrated NOAA observations imply for H_2 emission and soil uptake.~~ BASE model run.

3.2 ~~Emissions~~

3.1.1 Emission

~~Following Ghosh et al. (2015), the changes in the H_2 source ($\Delta S(H_2)$) needed to reduce the model bias ($\Delta H_2(sfc)$) can be estimated as:~~

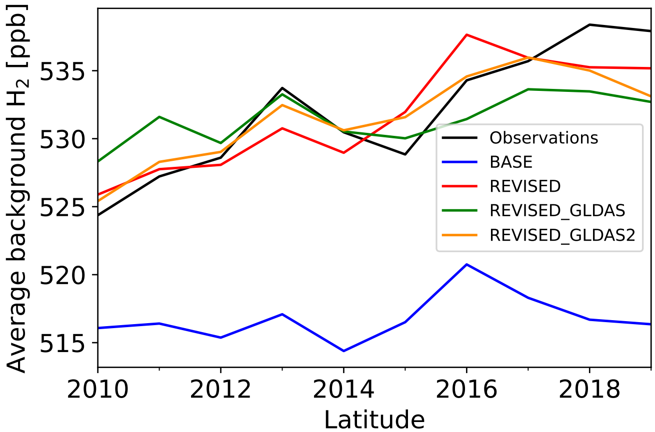

Figure 5. Mean observed and simulated H_2 at background sites (see Fig. 2 for locations)

$$\Delta S(\mathrm{H_2}) = K_1 \frac{d(\Delta \mathrm{H_2}(sfc))}{dt} + K_2 \Delta \mathrm{H_2}(sfc)$$

where K_1 is the ratio of the H_2 burden to the surface concentration of H_2, K_2 is the ratio of the loss of hydrogen to the surface concentration of H_2, and $\Delta H_2(sfc)$ is the difference between observed and simulated H_2 at background sites Fig. 5 shows that the BASE run exhibits a 10-15 ppb negative bias and fails to capture the $\simeq$ 15 ppb increase over the 2010–2019 period (Fig. 5). Equation ?? yields an estimated From this bias, we estimate a missing source of H_2 of $\simeq$ 2-2.5 Tg/yr circa 2010 and 3-4 Tg/yr circa 2019. The inferred increase in 2019 (Text S1.1). Similarly, Derwent et al. (2023) recently reported that a missing H_2 emissions over the 2010–2019 is of similar magnitude to the decline in anthropogenic emissions in our BASE simulation (Fig. 1)and we focus on this term in this section.

In the BASE simulation, $\simeq$ 80% of H_2 emission originate from the transportation and residential sectors (Fig. ??a). Global anthropogenic emissions are 1.4 source (5 Tg/yr lower in 2019 compared to 2010, with the largest decline from the transportation (-1 Tg/yr) and industrial (-0.4 Tg/yr) sectors, respectively. Fig. ??b shows a revised anthropogenic inventory for in 2020) was required to explain the observed increase in H_2 , which is described in Appendix ??. The revised inventoryincorporates a more detailed treatment of transportation and industrial emissions. In particular, we include concentration at Mace Head and Cape Grim since 2010.

Figs 5 and 6 show that the observed increase in H_2 leakage from industrial production can be well captured with the REVISED emission inventory. In this inventory, the increase in the missing source of H_2 for refining, ammonia, methanol and steel production, assuming a time-invariant leakage rate of 2%, consistent with recent estimates (2.7% (Fan et al., 2022), 1.2% (Arrigoni and Bravo Diaz, 2022)). We estimate that the increase in is explained by a lower decrease in anthropogenic H_2 demand from these sectors (+$\simeq$ 18 emissions associated with fossil fuel combustion (0.9 Tg/yr lower in 2019 relative to 2010 (International Energy Agency, 2019)) has resulted in $\simeq$0.3 compared to 1.6 Tg/yr more H_2 emissions over the 2010-2019 period. The REVISED anthropogenic emissions are estimated to be 14.1 Tg/yr in 2010 and 13.5 Tg/yr in 2019, a lower decrease than in the BASE configuration, which is consistent with the missing emissions inferred from equation ??. However, the updated treatment of anthropogenic emissions does not explain the low bias in the simulated the BASE inventory) and an increase in H_2 mixing ratio. Ehhalt and Rohrer (2009) surveyed many "minor" sources of emissions associated with H_2 , the combined magnitude of which could amount to 2 industrial usage (0.3 Tg/yr. For instance, we do not include geological sources of H_2, the magnitude of which carries considerable uncertainty (0-30 Tg/yr(Zgonnik, 2020)). In the REVISED simulation, we). We also increase the H_2 soil source from 3 Tg/yr to 4.5 Tg/yr as described in Appendix ??. Clearly more observational constraints are needed to develop a more robust to reduce the model negative bias. This change is well within the large uncertainties in the minor H_2 emission inventory.

We find that the REVISED configuration exhibits reduced mean biasagainst observations for both the mean (Fig. 2) and the trend (Figs 6 and 5). In contrast, the simulated North-South gradient (Fig. 2) and the H_2 seasonal cycle (Fig. 3) exhibit little sensitivity to the change in emissions.

Sectorial H_2 anthropogenic emissions in the BASE (a) and REVISED (b) configuration

Same as Fig. 4 but for the REVISED configuration

3.2 Deposition

In the previous subsection, we explored how changes in H_2 sources impact the model bias. In this section, we focus on the representation of the soil removal surveyed by Ehhalt and Rohrer (2009). In particular, it is a small fraction of the estimated geological source of H_2 , the largest sink of atmospheric H_2(23±7 Tg/yr (Zgonnik, 2020)), which we do not account for here.

The soil removal of REVISED emission inventory provides a possible explanation for the observed increase in atmospheric $H_2$is controlled by the activity of high-affinity hydrogen oxidizing bacteria (HA-HOB, Constant et al. (2010)). While considerable progress has been made in the last decade to characterize these organisms (Greening et al., 2015), their representation in global models remains simplistic (Paulot et al., 2021). . It highlights the importance of constraining H_2 uptake has been shown to be very sensitive to soil moisture (Smith-Downey et al., 2006). This reflects the competition between the biological uptake of emissions associated with H_2 , which tends to increase with soil moisture and the diffusion of H_2, which decreases with soil moisture (Bertagni et al., 2021). Furthermore, H_2 uptake has been shown to be inhibited when soil moisture is very low (Smith-Downey et al., 2006; Ehhalt and Rohrer, 2011)industrial use, a sector that is expected to grow rapidly in coming decades.

3.1.1 Deposition

To quantify possible changes in the soil removal of H_2 over the 2010-2019 period, we perform additional simulations using 3-hourly soil moisture and soil temperature from the NASA Global Land Data Assimilation System (Rodell et al., 2004) as described in Appendix ??. As in the BASE configuration, the deposition parameterization follows (Ehhalt and Rohrer, 2013) except for the parameterization of the soil moisture response of HA-HOB activity, which follows Bertagni et al. (2021). The parameterization of Bertagni et al. (2021) relates the minimum moisture threshold required for H_2 uptake by HA-HOB to soil

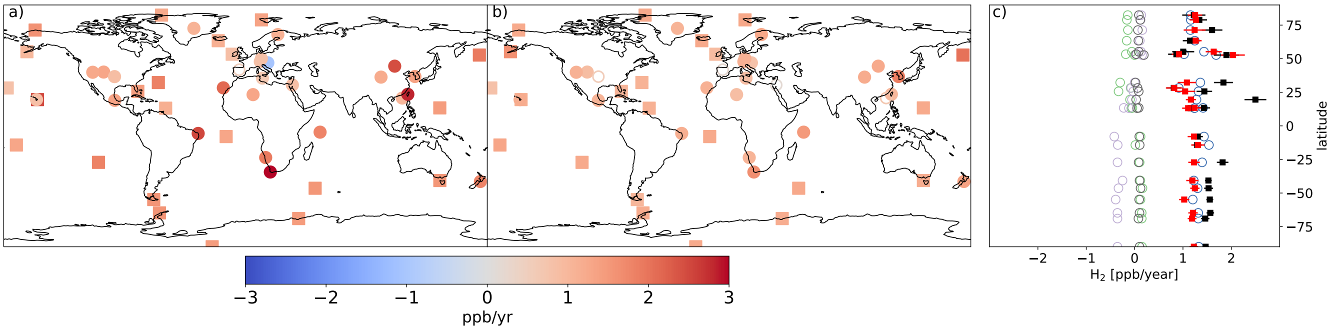

Figure 6. Same as Fig. 4 but for the REVISED configuration

~~hydrological properties, which facilitates its incorporation in global models. Here, we assume that H_2 uptake is inhibited when the soil matrix potential is lower than $\Psi_{ws} = -3000 kPa$ (Bertagni et al., 2021). This configuration, including the REVISED emissions, is referred to as REVISED_GLDAS hereafter (Table 1)~~ The BASE and REVISED experiments assume no interannual variability in $v_d(H_2)$. However, we have recently shown that climate change may cause an increase in $v_d(H_2)$ (Paulot et al., 2021). Recent analysis of observations at Mace Head also suggests that $v_d(H_2)$ has increased in recent decades (Derwent et al., 2021).

Fig. 7 shows that the ~~resulting~~ REVISED_GLDAS and REVISED_GLDAS2 $v_d(H_2)$ ~~exhibits a different meridional distribution~~ exhibit different meridional distributions relative to the BASE configuration with faster removal in the subtropics and northern high latitudes but slower removal in the tropics. This reflects more efficient removal of ~~hydrogen~~ H_2 in arid regions and slower removal in ~~tropical savanna than in the BASE configuration .~~ the tropics. These spatial differences are the largest for the REVISED_GLDAS2 configuration due to the activation of HA-HOB at a lower soil moisture. Fig. 7b further shows that $v_d(H_2)$ in the REVISED_GLDAS ~~increases from 2009 to 2019~~ and REVISED_GLDAS2 configuration both increase over the 2010-2019 period in the Northern mid latitudes. This increase reflects drier and warmer conditions in Europe, the Western US as well as parts of Siberia, which result in faster biological uptake rates and promote H_2 diffusivity (Fig. ~~??~~S5). This mechanism may ~~explain~~ contribute to the reported 1.2%/yr increase in H_2 deposition velocity at Mace Head from 1994 to 2020 (Derwent et al., 2021). ~~In contrast, drier~~ Drier conditions in Australia ~~and in the Northern subtropics~~ trigger biotic limitations, which results in a large decrease in H_2 deposition velocity in ~~ther~~ the Southern mid latitudes in the REVISED_GLDAS configuration. In contrast, we find no significant suppression of H_2 uptake in Australia over this time period in the the REVISED_GLDAS2 configuration due a lower threshold for biotic limitation.

Changes to the spatial distribution of $v_d(H_2)$ and the increase in H_2 removal in the Northern mid latitudes (Fig. 7b) in REVISED_GLDAS result in a larger pole-to-pole difference in surface H_2 (Fig. 2) and a reduction in the simulated trend (Fig. 8) in the Northern mid to high latitudes. Both of these changes tend to degrade the model performance relative to the REVISED configuration. In contrast, the REVISED_GLDAS configuration better captures the timing of the H_2 maximum in the northern hemisphere (clusters 3 and 4, Fig. 3~~).~~a).

~~Experimental studies have shown that HA-HOB are present in very arid environments and strongly stimulated by wetting (Jordaan et al., 2020). However, the soil moisture required for H_2 uptake remains poorly constrained. We thus conduct a range of sensitivity simulations to systematically test the dependence~~ Systematic assessment of the sensitivity of $v_d(\mathrm{H_2})$ to Ψ_{ws} ~~(see Appendix ??).~~ and the strength of the litter barrier is shown in Fig. 9~~a shows~~ . We find that a lower soil moisture threshold for HA-HOB activation (i.e., a lower Ψ_{ws}) favors H_2 removal in the Northern hemisphere relative to the Southern hemisphere (Fig. 9a) and results in a larger increase in $v_d(\mathrm{H_2})$ over the ~~2009–2019~~ 2010–2019 period (Fig. 9b), especially in the Southern hemisphere (Fig. 9c). This suggests that a lower Ψ_{ws} would tend to worsen the model performance in the absence of a litter barrier (given the REVISED emissions).

~~Previous studies have also shown that~~ The litter barrier tends to increase the importance of arid regions for H_2 ~~uptake by HA-HOB can be reduced by litter (Smith-Downey et al., 2008; Ehhalt and Rohrer, 2009), which acts as a barrier for the diffusion of~~ removal. This makes H_2 ~~to active sites. We find that such a~~ uptake more susceptible to moisture inhibition, such that a stronger litter barrier tends to ~~increase the~~ result in a lower increase of even a decrease in $v_d(\mathrm{H_2})$ over the 2010-2019 period. Under all scenarios, the litter barrier tends to increase the gradient in $v_d(\mathrm{H_2})$ between Northern and Southern ~~hemisphere (Fig. 9a) and to reduce (or even reverse) the increase in $v_d(\mathrm{H_2})$ (Fig. 9b).~~ hemispheres.

It is notable that no configuration results in little change in $v_d(\mathrm{H_2})$ without producing large and increasing gradients between the Northern and Southern ~~hemisphere~~hemispheres. As a result, our model cannot ~~reproduce~~ capture the observed trends, meridional gradient, and seasonality together given our ~~best~~ REVISED estimate of H_2 emissions~~(REVISED configuration)~~. This is illustrated by the REVISED_GLDAS2 configuration ~~in which we use a lower moisture threshold~~ (Ψ_{ws}=-10000 kPa~~) and account for both the impact of litter and canopy on H_2 soil uptake (Litter~~, Litter_scale=1)~~. This configuration~~ , which is found to improve the simulated trend relative to the REVISED_GLDAS (not shown) and the simulated seasonality relative to the REVISED configuration (Fig. 3) but results in a ~~larger~~ large overestimate of the South/North meridional gradient ~~than the REVISED_GLDAS configuration~~ (Fig. 2).

This highlights the need for a more detailed representation of the factors that modulate ~~HA-HOB (Khdhiri et al., 2015)~~ $v_d(\mathrm{H_2})$ (Khdhiri et al., 2015) to help interpret changes in H_2 concentrations.

~~Same as Fig. 4 but for the REVISED_GLDAS configuration~~

4 Conclusions

The recently released H_2 dry air mole fraction measurements from the NOAA Global Cooperative Air Sampling Network expand the spatial coverage of the WMO Global Atmospheric Watch observations. This offers the opportunity to assess the representation of the H_2 atmospheric budget in the state-of-the-art GFDL-AM4.1 global atmospheric chemistry climate model. Observations show that H_2 has increased on average by 1 to 2 ~~ppbv~~ppb/year over the 2010-2019 period. This change can be explained by the increase in photochemically-produced H_2 (mostly from CH_4) provided direct anthropogenic H_2 emissions have remained stable during this time period. We hypothesize that this stability reflects the compensation between declining emissions associated with fossil fuel combustion (mostly from the transport sector) and increasing emissions associated with

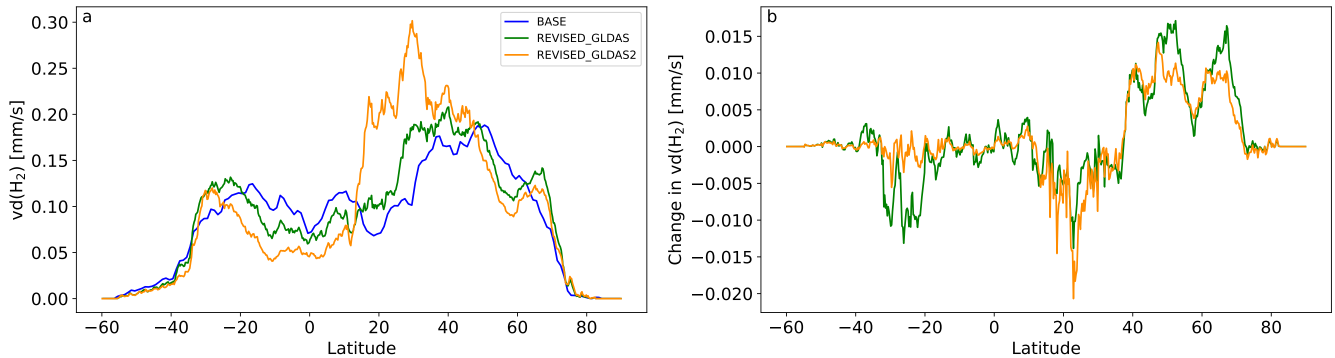

Figure 7. Meridional distribution of $v_d(H_2)$ in the BASE, REVISED_GLDAS, and REVISED_GLDAS2 simulations (a) and (b) simulated change in $v_d(H_2)$ between (~~2015–2019~~2017–2019) and (~~2009–2013~~2010-2012)

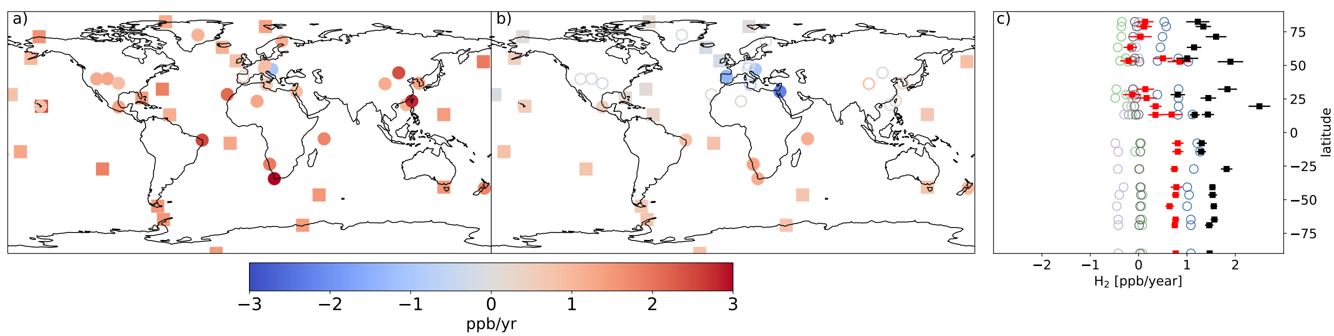

Figure 8. Same as Fig. 4 but for the REVISED_GLDAS configuration

H_2-producing facilities (~~primarily for ammonia (NH_3) and methanol production as well as refineries~~for refining, ammonia, methanol and steel production). This is notable as H_2 release from H_2 production facilities is poorly understood yet ~~critical~~ important to assess the climate benefits of H_2 (Hauglustaine et al., 2022; Bertagni et al., 2022).

We show that the observed trend, seasonality, and meridional gradient of H_2 provide complementary constraints on the global H_2 biogeochemical cycle. We find that our model fails to capture all three constraints together, which likely reflects fundamental gaps in our representation of the soil removal of H_2 by microorganisms (HA-HOB). ~~In particular, we find that the sign of the simulated global trend in soil~~ Such uncertainties are important as an increase in $v_d(H_2)$ would require a commensurate increase in H_2 ~~removal over the 2010–2019 period is sensitive to the soil moisture threshold below which the activity of HA-HOB is suppressed~~sources to explain the observed change in H_2 concentration.

This study highlights the need for coordinated field and laboratory data collection efforts to help improve models of the distribution and activity of HA-HOB in global models (American Academy of Microbiology, 2023). Such ~~efforts are currently hindered by the lack of sensors that offer higher time resolution and maintain good sensitivity and stable response. Such efforts are~~ work is critical to quantify the response of atmospheric H_2 to increasing anthropogenic H_2 usage as well as hydrological

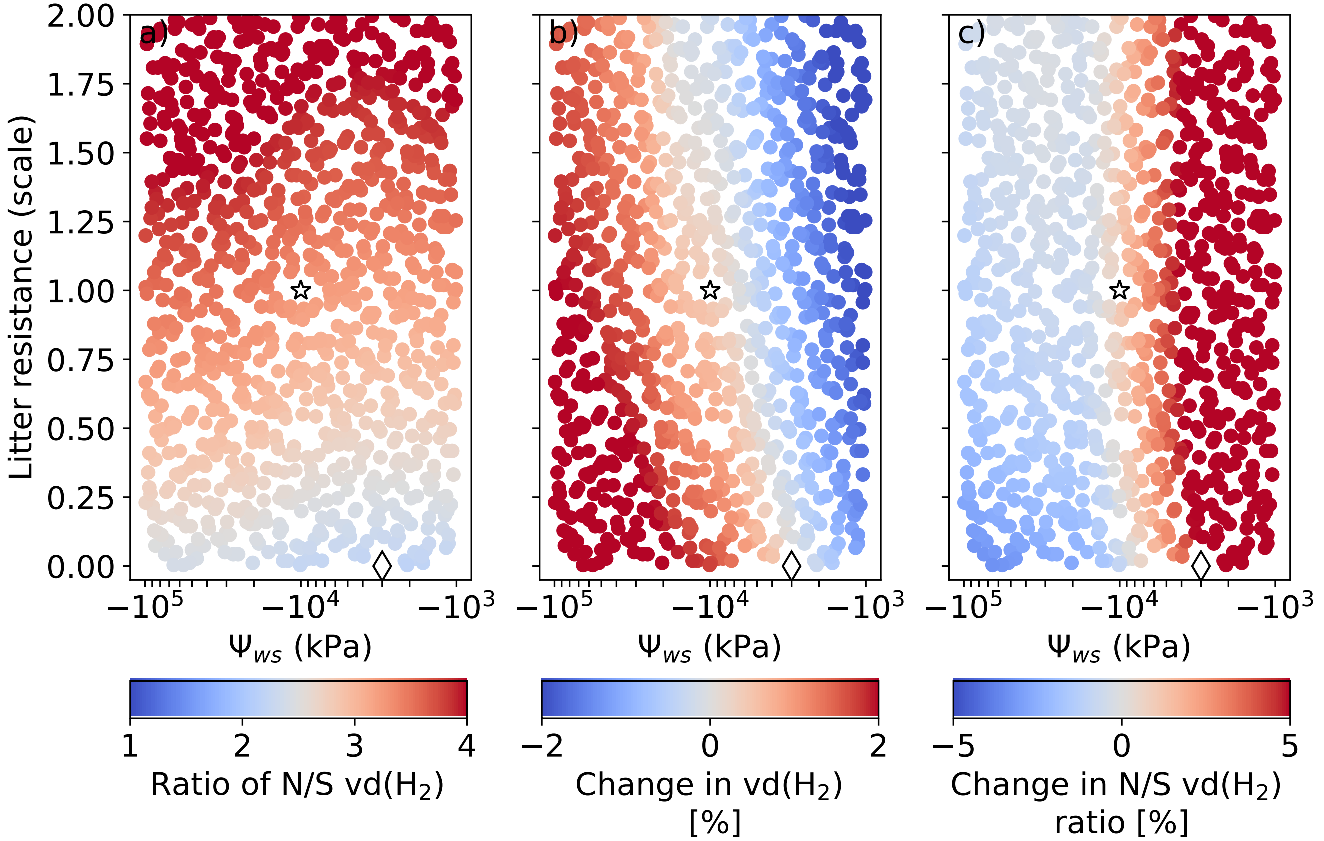

Figure 9. Simulated sensitivity of $v_d(\mathrm{H_2})$ to Ψ_{ws} and the strength of the litter diffusive barrier. Panels a, b and c show the response of the North/South ratio of $v_d(\mathrm{H_2})$, the difference in $v_d(\mathrm{H_2})$ in (~~2015–2019~~2017–2019) relative to (~~2009-2013~~2010-2012), and the difference in the N/S $v_d(\mathrm{H_2})$ gradient in (~~2015–2019~~2017–2019) relative to (~~2009-2013~~2010-2012), respectively. The REVISED_GLDAS configuration uses $\Psi_{ws} = -3000$ kPa and no litter resistance (diamond). The REVISED_GLDAS2 uses $\Psi_{ws} = -10000$ kPa and ~~a litter resistance~~ the default (scale~~of~~ =1) litter resistance (star). The litter scale reflects the perturbation to the default litter resistance (see Text S1.4)

changes associated with climate change (Jansson and Hofmockel, 2019; Huang et al., 2015) but is hindered by the lack of sensors that offer higher time resolution and maintain good sensitivity and stable response.

Code and data availability. The code for the GFDL ESM4.1 model is available at https://zenodo.org/record/3836405. NOAA Global Cooperative Network Flask Air H_2 (Pétron et al., 2023) can be downloaded at https://doi.org/10.15138/WP0W-EZ08.

Appendix A: Revised emission inventory

The H_2 budget in the REVISED experiment is summarized in Fig. ??. Anthropogenic and natural emissions are described below.

1 Anthropogenic emissions

Sector-based molar H_2 to CO emission ratio

BASE[a] REVISED Industrial 0.2 0.2 Residential Biofuel 0.3 0.31 [b] Other 0.3 0 [c] Transportation Gasoline-powered vehicles (up to EURO3) 0.5 0.5 [d] Gasoline-powered vehicles (EURO4 and above) 0.5 1 [d] Diesel-powered vehicle 0.5 0.0021 [d] CNG-powered vehicle 0.5 0.04 [d] Waste 0.07 0.32 [b] [a] Paulot et al. (2021) [b] Andreae (2019) [c] Vollmer et al. (2012) [d] Bond et al. (2010, 2011

In the BASE simulation, anthropogenic emissions are assumed to solely originate from combustion processes and calculated using time-invariant and source-specific H_2 to CO emission ratios (Table ??) that reflect the water–gas shift reaction.

The REVISED emission inventory incorporates a more detailed treatment of H_2 emission factors. In particular, we account for the difference between gasoline- and diesel-powered vehicles and for the increase in the H_2 to CO emission ratio associated with three-way catalytic converters (Bond et al., 2010, 2011). H_2 vehicular emissions are estimated using H_2:CO emissions ratio (Table ??) and ECLIPSEv6 CO region- and vehicle-type specific emissions (Klimont et al., 2017). These changes result in a model decrease in transportation emissions in 2010 (5.5 Tg/yr vs 5.8 Tg/yr).The REVISED emission ratio for biofuel and waste are from Andreae (2019). Following Vollmer et al. (2012), we assume that other residential emissions of CO (e.g., oil and gas stoves) do not produce H_2.

The industrial emission ratio is not modified between the BASE and REVISED emissions inventories. However, in the REVISED inventory, we use the Emissions Database for Global Atmospheric Research (EDGAR) v6.1 industrial CO emissions instead of CEDS to estimate industrial H_2 emissions. These inventories exhibit different trends for CO (+8.7 Tg/yr for EDGAR and -30.7 TgTg/yr for CEDS in 2018 relative to 2010), which translate to different trends in H_2 emissions (+0.1 Tg/yr and -0.4 TgTg/yr, respectively). We select the EDGAR inventory as we identified the decrease in industrial H_2 as one of the main drivers for the decline in anthropogenic emission in the BASE inventory.

The REVISED inventory also includes a non-combustion source of H_2 associated with H_2 industrial production (primarily for NH_3 production and refining (International Energy Agency, 2019)). Using a 2% release rate (Bond et al., 2010) yields an estimated source of 1.5 Tg/yr in 2010 and 1.8 Tg/yr in 2019. The increase in H_2 thus contributes the largest increase in H_2 emissions over the 2010 to 2019, which highlights the need to better quantify H_2 leakage throughout the H_2 supply chain.

1 Natural emissions

The magnitude of natural emissions in the BASE configuration (9 Tg/yr) is similar to that of anthropogenic emissions ($\simeq$ 13 Tg/yr) with considerable uncertainties (Ehhalt and Rohrer, 2009). In the BASE configuration, soil and ocean emissions are 3 and 6 Tg/yr respectively (Ehhalt and Rohrer, 2009) and are distributed based on the soil and marine CO emission patterns in the Precursors of Ozone and their Effects in the Troposphere inventory (Granier et al., 2005).

In the REVISED inventory, marine H_2 emissions are calculated interactively (Johnson, 2010; Paulot et al., 2021) from the simulated distribution of surface seawater CO (Conte et al., 2019), scaled to produce a net flux of 6 Tg/yr. We use CO as a proxy for biological activity following Pieterse et al. (2011). Relative to the BASE inventory, the REVISED inventory exhibits higher emissions in the tropics and lower emissions in the Southern ocean, which reflects changes in the solubility of H_2 (Fig. **??**a).

The soil source of H_2 is distributed following the simulated land biological nitrogen fixation from the MIROC-ES2L Earth system model (Hajima et al., 2020). The soil H_2 flux is set to 4.5 Tg/yr, which is at the high end of previous estimates (Ehhalt and Rohrer, 2009). MIROCA-ES2L explicitly accounts for biological nitrogen fixation by crops. This results in much larger H_2 emissions in the Northern mid latitudes relative to the BASE soil emissions.

Biomass burning emissions are kept unchanged from Paulot et al. (2021). However, we note that using the emission factors of Andreae (2019) would reduce H_2 emissions from 8.3 to 6.1 Tg/yr over the 2010–2019 period.

Appendix A: Deposition sensitivity

The deposition velocity of H_2 can be expressed as

$$\frac{1}{v_d(\mathrm{H_2})} = \frac{1}{g_i} + \frac{1}{g_s}$$

where g_i and g_s represent the H_2 conductance through barriers that reduce the transport of H_2 to active sites (e.g., canopy, litter, ...) and in the soil.

The conductance in the soil is expressed after Ehhalt and Rohrer (2013) as

$$g_s = \sqrt{k_m\, hT\, f\, D_s}$$

where hT and f are the sensitivity of H_2 biological uptake to temperature and soil moisture, respectively, D_s is the moisture-dependent diffusivity of H_2 in the soil, and k_m represents the maximum uptake rate of H_2. All moisture dependencies are evaluated after Bertagni et al. (2021). Namely, f is expressed as

$$f(s) = \frac{1}{N}(s - s_{ws})^{\beta_1}(1 - s_{ws})^{\beta_2}$$

where s_{ws} is the threshold below which H_2 consumption is inhibited. s_{ws} can be estimated as:

$$s_{ws} = \left(\frac{\tilde{\Psi}}{\Psi_{ws}} \right)^{\frac{1}{b}}$$

where the $\tilde{\Psi}$ and b constants can be determined experimentally (Bertagni et al., 2021) and Ψ_{ws} is the soil matrix potential below which bacterial uptake is inhibited. Given s_{ws}, β_1 and β_2 can be estimated based on observational constraints (Bertagni et al., 2021) .

For g_l, we account for the impact of canopy and above-ground litter. For the canopy, we assume a time-invariant conductance based on the vegetation type (Makar et al., 2018). The litter conductance is estimated assuming a litter porosity of 0.62 (Wang et al., 2019). The litter depth is estimated based on the simulated above ground carbon from the IPSL INCA model historical simulation (Boucher et al., 2021) assuming a density of 0.03 g/cm^3 (Chojnacky et al., 2009).

We carry sensitivity experiments in which the resistance due to litter and canopy conductance are scaled by a factor between 0 and 2 and Ψ_{ws} takes values between -10^5 and -10^3 kPa (compared to -3000 kPa in REVISED_GLDAS). For each combination, k_m is optimized to yield the same global $v_d(H_2)$ for year 2010. We find that the canopy resistance has little impact on the meridional gradient and trend and we focus our analysis on the litter resistance.

Same as Fig. 1 for the REVISED experiment. Marine and soil H_2 emissions in the BASE and REVISED emission inventories. Changes in snow depth (a), soil temperature (b), soil moisture (as a fraction of pores (c)) and their impact on H_2 soil diffusivity (d), H_2 bacterial uptake, (e) and H_2 deposition velocity (REVISED_GLDAS, panel f) between years (2015–2019) and years (2009–2012).

Author contributions. FP designed the research, developed, and analyzed the model simulations. GP and AC collected and processed H_2 observations from the NOAA network and provided guidance regarding their interpretation. MB developed the soil moisture parameterization of HA-HOB used in the REVISED_GLDAS and REVISED_GLDAS2 configurations. All authors contributed to the drafting of the manuscript.

Competing interests. None

Acknowledgements. We thank Vaishali Naik for her help with generating model-ready H_2 emissions. We thank Larry Horowitz, Vaishali Naik, Amilcare Porporato, and Xinning Zhang for their helpful comments on the manuscript. This research was supported in part by NOAA cooperative agreements NA17OAR4320101 and NA22OAR4320151 and by the U.S. Department of Energy, Office of Energy Efficiency and Renewable Energy (EERE), specifically the Hydrogen and Fuel Cell Technologies Office. The views expressed herein do not necessarily represent the views of the U.S. Department of Energy or the United States Government.

References

Abe, J., Popoola, A., Ajenifuja, E., and Popoola, O.: Hydrogen energy, economy and storage: Review and recommendation, International Journal of Hydrogen Energy, 44, 15 072–15 086, https://doi.org/10.1016/j.ijhydene.2019.04.068, 2019.

Akagi, S. K., Yokelson, R. J., Wiedinmyer, C., Alvarado, M. J., Reid, J. S., Karl, T., Crounse, J. D., and Wennberg, P. O.: Emission factors for open and domestic biomass burning for use in atmospheric models, Atmos. Chem. Phys., 11, 4039–4072, https://doi.org/10.5194/acp-11-4039-2011, 2011.

American Academy of Microbiology: Microbes in Models: Integrating Microbes into Earth System Models for Understanding Climate Change: Report on an American Academy of Microbiology Virtual Colloquium held on Dec. 6 and 8, 2022 Washington (DC), 2023.

Andreae, M. O.: Emission of trace gases and aerosols from biomass burning – an updated assessment, Atmospheric Chemistry and Physics, 19, 8523–8546, https://doi.org/10.5194/acp-19-8523-2019, 2019.

Arrigoni, A. and Bravo Diaz, L.: Hydrogen emissions from a hydrogen economy and their potential global warming impact: summary report of the Clean Hydrogen Joint Undertaking expert workshop on the Environmental Impacts of Hydrogen, JRC130362, https://doi.org/10.2760/065589, 2022.

Arthur, D. and Vassilvitskii, S.: K-means++: The advantages of careful seeding, Proceedings of the eighteenth annual ACM-SIAM symposium on discreate algorithm, 2007.

Bay, S. K., Dong, X., Bradley, J. A., Leung, P. M., Grinter, R., Jirapanjawat, T., Arndt, S. K., Cook, P. L. M., LaRowe, D. E., Nauer, P. A., Chiri, E., and Greening, C.: Trace gas oxidizers are widespread and active members of soil microbial communities, Nature Microbiology, 6, 246–256, https://doi.org/10.1038/s41564-020-00811-w, 2021.

Bertagni, M. B., Paulot, F., and Porporato, A.: Moisture Fluctuations Modulate Abiotic and Biotic Limitations of H_2 Soil Uptake, Global Biogeochemical Cycles, 35, https://doi.org/10.1029/2021gb006987, 2021.

Bertagni, M. B., Pacala, S. W., Paulot, F., and Porporato, A.: Risk of the hydrogen economy for atmospheric methane, Nature Communications, 13, https://doi.org/10.1038/s41467-022-35419-7, 2022.

Bond, S., Alvarez, R., Vollmer, M., Steinbacher, M., Weilenmann, M., and Reimann, S.: Molecular hydrogen (H2) emissions from gasoline and diesel vehicles, Science of The Total Environment, 408, 3596–3606, https://doi.org/10.1016/j.scitotenv.2010.04.055, 2010.

Bond, S., Gül, T., Reimann, S., Buchmann, B., and Wokaun, A.: Emissions of anthropogenic hydrogen to the atmosphere during the potential transition to an increasingly H_2-intensive economy, International Journal of Hydrogen Energy, 36, 1122–1135, https://doi.org/10.1016/j.ijhydene.2010.10.016, 2011.

Boucher, O., Denvil, S., Levavasseur, G., Cozic, A., Caubel, A., Foujols, M.-A., Meurdesoif, Y., Balkanski, Y., Checa-Garcia, R., Hauglustaine, D., Bekki, S., and Marchand, M.: IPSL IPSL-CM6A-LR-INCA model output prepared for CMIP6 CMIP historical, https://doi.org/10.22033/ESGF/CMIP6.13601, 2021.

Chojnacky, D., Amacher, M., and Gavazzi, M.: Separating Duff and Litter for Improved Mass and Carbon Estimates, Southern Journal of Applied Forestry, 33, 29–34, https://doi.org/10.1093/sjaf/33.1.29, 2009.

Constant, P., Poissant, L., and Villemur, R.: Isolation of Streptomyces sp. PCB7, the first microorganism demonstrating high-affinity uptake of tropospheric H_2, The ISME Journal, 2, 1066–1076, https://doi.org/10.1038/ismej.2008.59, 2008.

Constant, P., Chowdhury, S. P., Pratscher, J., and Conrad, R.: Streptomycetes contributing to atmospheric molecular hydrogen soil uptake are widespread and encode a putative high-affinity [NiFe]-hydrogenase, Environmental Microbiology, 12, 821–829, https://doi.org/10.1111/j.1462-2920.2009.02130.x, 2010.

Conte, L., Szopa, S., Séférian, R., and Bopp, L.: The oceanic cycle of carbon monoxide and its emissions to the atmosphere, Biogeosciences, 16, 881–902, https://doi.org/10.5194/bg-16-881-2019, 2019.

da Silva Veras, T., Mozer, T. S., da Costa Rubim Messeder dos Santos, D., and da Silva César, A.: Hydrogen: Trends, production and characterization of the main process worldwide, International Journal of Hydrogen Energy, 42, 2018–2033, https://doi.org/10.1016/j.ijhydene.2016.08.219, 2017.

Dawood, F., Anda, M., and Shafiullah, G.: Hydrogen production for energy: An overview, International Journal of Hydrogen Energy, 45, 3847–3869, https://doi.org/10.1016/j.ijhydene.2019.12.059, 2020.

Derwent, R. G.: Global warming potential (GWP) for hydrogen: Sensitivities, uncertainties and meta-analysis, International Journal of Hydrogen Energy, https://doi.org/10.1016/j.ijhydene.2022.11.219, 2022.

Derwent, R. G., Collins, W. J., Johnson, C. E., and Stevenson, D. S.: Transient Behaviour of Tropospheric Ozone Precursors in a Global 3-D CTM and Their Indirect Greenhouse Effects, Climatic Change, 49, 463–487, https://doi.org/10.1023/a:1010648913655, 2001.

Derwent, R. G., Simmonds, P. G., Doherty, S. J. O., Spain, T. G., and Young, D.: Natural greenhouse gas and ozone-depleting substance sources and sinks from the peat bogs of Connemara, Ireland from 1994–2020, Environmental Science: Atmospheres, 1, 406–415, https://doi.org/10.1039/d1ea00040c, 2021.

Derwent, R. G., Simmonds, P. G., O'Doherty, S., Manning, A. J., and Spain, T. G.: High-frequency, continuous hydrogen observations at Mace Head, Ireland from 1994 to 2022: Baselines, pollution events and 'missing' sources, Atmospheric Environment, 312, 120 029, https://doi.org/10.1016/j.atmosenv.2023.120029, 2023.

Dunne, J. P., Horowitz, L. W., Adcroft, A. J., Ginoux, P., Held, I. M., John, J. G., Krasting, J. P., Malyshev, S., Naik, V., Paulot, F., Shevliakova, E., Stock, C. A., Zadeh, N., Balaji, V., Blanton, C., Dunne, K. A., Dupuis, C., Durachta, J., Dussin, R., Gauthier, P. P. G., Griffies, S. M., Guo, H., Hallberg, R. W., Harrison, M., He, J., Hurlin, W., McHugh, C., Menzel, R., Milly, P. C. D., Nikonov, S., Paynter, D. J., Ploshay, J., Radhakrishnan, A., Rand, K., Reichl, B. G., Robinson, T., Schwarzkopf, D. M., Sentman, L. T., Underwood, S., Vahlenkamp, H., Winton, M., Wittenberg, A. T., Wyman, B., Zeng, Y., and Zhao, M.: The GFDL Earth System Model version 4.1 (GFDL-ESM 4.1): Overall coupled model description and simulation characteristics, Journal of Advances in Modeling Earth Systems, https://doi.org/10.1029/2019ms002015, 2020.

Ehhalt, D. and Rohrer, F.: Deposition velocity of H_2: a new algorithm for its dependence on soil moisture and temperature, Tellus B: Chemical and Physical Meteorology, 65, 19 904, https://doi.org/10.3402/tellusb.v65i0.19904, 2013.

Ehhalt, D. H. and Rohrer, F.: The tropospheric cycle of H_2: a critical review, Tellus B: Chemical and Physical Meteorology, 61, 500–535, https://doi.org/10.1111/j.1600-0889.2009.00416.x, 2009.

Ehhalt, D. H. and Rohrer, F.: The dependence of soil H_2 uptake on temperature and moisture: a reanalysis of laboratory data, Tellus B: Chemical and Physical Meteorology, 63, 1040–1051, https://doi.org/10.1111/j.1600-0889.2011.00581.x, 2011.

Fan, Z., Sheerazi, H., Bhardwaj, A., Corbeau, A.-S., Longobardi, K., Castañeda, A., Merz, A.-K., Woodall, C. M., Agrawal, M., Orozco-Sanchez, S., and Friedmann, J.: Hydrogen Leakage: A Hydrogen Leakage: A Potential Risk for the Hydrogen Economy, https://www.energypolicy.columbia.edu/publications/hydrogen-leakage-potential-risk-hydrogen-economy/, 2022.

Francey, R. J., Steele, L. P., Spencer, D. A., Langenfelds, R. L., Law, R. M., Krummel, P. B., Fraser, P. J., Etheridge, D. M., Derek, N., Coram, S. A., Cooper, L. N., Allison, C. E., Porter, L., and Baly, S.: The CSIRO (Australia) measurement of greenhouse gases in the global atmosphere., Tech. rep., http://hdl.handle.net/102.100.100/191835?index=1, 2003.

Ghosh, A., Patra, P. K., Ishijima, K., Umezawa, T., Ito, A., Etheridge, D. M., Sugawara, S., Kawamura, K., Miller, J. B., Dlugokencky, E. J., Krummel, P. B., Fraser, P. J., Steele, L. P., Langenfelds, R. L., Trudinger, C. M., White, J. W. C., Vaughn, B., Saeki, T., Aoki, S., and

Nakazawa, T.: Variations in global methane sources and sinks during 1910–2010, Atmospheric Chemistry and Physics, 15, 2595–2612, https://doi.org/10.5194/acp-15-2595-2015, 2015.

Global Monitoring Laboratory: Carbon Cycle Gases observation sites, https://www.gml.noaa.gov/dv/site/?program=ccgg, 2023.

Granier, C., Lamarque, J. F., Mieville, A., Müller, J. F., Olivier, J., Orlando, J., Peters, J., Petron, G., Tyndall, G., and Wallens, S.: POET, a database of surface emissions of ozone precursors, available on internet at http://www.aero.jussieu.fr/projet/ACCENT/POET.php, Tech. rep., 2005.

Grant, A., Archibald, A. T., Cooke, M. C., Nickless, G., and Shallcross, D. E.: Modelling the oxidation of 15 VOCs to track yields of hydrogen, Atmospheric Science Letters, 11, 265–269, https://doi.org/10.1002/asl.286, 2010.

Greening, C. and Grinter, R.: Microbial oxidation of atmospheric trace gases, Nature Reviews Microbiology, 20, 513–528, https://doi.org/10.1038/s41579-022-00724-x, 2022.

Greening, C., Constant, P., Hards, K., Morales, S. E., Oakeshott, J. G., Russell, R. J., Taylor, M. C., Berney, M., Conrad, R., and Cook, G. M.: Atmospheric Hydrogen Scavenging: from Enzymes to Ecosystems, Applied and Environmental Microbiology, 81, 1190–1199, https://doi.org/10.1128/aem.03364-14, 2015.

Guenther, A., Karl, T., Harley, P., Wiedinmyer, C., Palmer, P. I., and Geron, C.: Estimates of global terrestrial isoprene emissions using MEGAN (Model of Emissions of Gases and Aerosols from Nature), Atmos. Chem. Phys., 6, 3181–3210, 2006.

Guenther, A. B., Jiang, X., Heald, C. L., Sakulyanontvittaya, T., Duhl, T., Emmons, L. K., and Wang, X.: The Model of Emissions of Gases and Aerosols from Nature version 2.1 (MEGAN2.1): an extended and updated framework for modeling biogenic emissions, Geoscientific Model Development, 5, 1471–1492, https://doi.org/10.5194/gmd-5-1471-2012, 2012.

Hajima, T., Watanabe, M., Yamamoto, A., Tatebe, H., Noguchi, M. A., Abe, M., Ohgaito, R., Ito, A., Yamazaki, D., Okajima, H., Ito, A., Takata, K., Ogochi, K., Watanabe, S., and Kawamiya, M.: Development of the MIROC-ES2L Earth system model and the evaluation of biogeochemical processes and feedbacks, Geoscientific Model Development, 13, 2197–2244, https://doi.org/10.5194/gmd-13-2197-2020, 2020.

Hauglustaine, D., Paulot, F., Collins, W., Derwent, R., Sand, M., and Boucher, O.: Climate benefit of a future hydrogen economy, Communications Earth & Environment, 3, https://doi.org/10.1038/s43247-022-00626-z, 2022.

Holladay, J., Hu, J., King, D., and Wang, Y.: An overview of hydrogen production technologies, Catalysis Today, 139, 244–260, https://doi.org/10.1016/j.cattod.2008.08.039, 2009.

Horowitz, L. W., Naik, V., Paulot, F., Ginoux, P. A., Dunne, J. P., Mao, J., Schnell, J., Chen, X., He, J., John, J. G., Lin, M., Lin, P., Malyshev, S., Paynter, D., Shevliakova, E., and Zhao, M.: The GFDL Global Atmospheric Chemistry-Climate Model AM4.1: Model Description and Simulation Characteristics, Journal of Advances in Modeling Earth Systems, https://doi.org/10.1029/2019ms002032, 2020.

Howarth, R. W. and Jacobson, M. Z.: How green is blue hydrogen?, Energy Science & Engineering, 9, 1676–1687, https://doi.org/10.1002/ese3.956, 2021.

Huang, J., Yu, H., Guan, X., Wang, G., and Guo, R.: Accelerated dryland expansion under climate change, Nature Climate Change, 6, 166–171, https://doi.org/10.1038/nclimate2837, 2015.

Hydrogen Council: Hydrogen scaling up. A sustainable pathway for the global energy transition, 2017.

International Energy Agency: The Future of Hydrogen – Seizing today's opportunities, Tech. rep., International Energy Agency, Paris, France, 2019.

International Energy Agency: Global Hydrogen Review 2022, Tech. rep., International Energy Agency, Paris, France, 2022.

Jansson, J. K. and Hofmockel, K. S.: Soil microbiomes and climate change, Nature Reviews Microbiology, 18, 35–46, https://doi.org/10.1038/s41579-019-0265-7, 2019.

Johnson, M. T.: A numerical scheme to calculate temperature and salinity dependent air-water transfer velocities for any gas, Ocean Sci., 6, 913–932, 2010.

Jordaan, K., Lappan, R., Dong, X., Aitkenhead, I. J., Bay, S. K., Chiri, E., Wieler, N., Meredith, L. K., Cowan, D. A., Chown, S. L., and Greening, C.: Hydrogen-Oxidizing Bacteria Are Abundant in Desert Soils and Strongly Stimulated by Hydration, mSystems, 5, https://doi.org/10.1128/msystems.01131-20, 2020.

Jordan, A. and Steinberg, B.: Calibration of atmospheric hydrogen measurements, Atmospheric Measurement Techniques, 4, 509–521, https://doi.org/10.5194/amt-4-509-2011, 2011.

Kalnay, E., Kanamitsu, M., Kistler, R., Collins, W., Deaven, D., Gandin, L., Iredell, M., Saha, S., White, G., Woollen, J., Zhu, Y., Leetmaa, A., Reynolds, R., Chelliah, M., Ebisuzaki, W., Higgins, W., Janowiak, J., Mo, K. C., Ropelewski, C., Wang, J., Jenne, R., and Joseph, D.: The NCEP/NCAR 40-Year Reanalysis Project, Bull. Am. Meteorol. Soc., 77, 437–471, 1996.

Khdhiri, M., Hesse, L., Popa, M. E., Quiza, L., Lalonde, I., Meredith, L. K., Röckmann, T., and Constant, P.: Soil carbon content and relative abundance of high affinity H_2-oxidizing bacteria predict atmospheric H_2 soil uptake activity better than soil microbial community composition, Soil Biology and Biochemistry, 85, 1–9, https://doi.org/10.1016/j.soilbio.2015.02.030, 2015.

Klimont, Z., Kupiainen, K., Heyes, C., Purohit, P., Cofala, J., Rafaj, P., Borken-Kleefeld, J., and Schöpp, W.: Global anthropogenic emissions of particulate matter including black carbon, Atmospheric Chemistry and Physics, 17, 8681–8723, https://doi.org/10.5194/acp-17-8681-2017, 2017.

Lapi, T., Chatzimpiros, P., Raineau, L., and Prinzhofer, A.: System approach to natural versus manufactured hydrogen: An interdisciplinary perspective on a new primary energy source, International Journal of Hydrogen Energy, 47, 21 701–21 712, https://doi.org/10.1016/j.ijhydene.2022.05.039, 2022.

Lefeuvre, N., Truche, L., Donzé, F., Ducoux, M., Barré, G., Fakoury, R., Calassou, S., and Gaucher, E. C.: Native H2 Exploration in the Western Pyrenean Foothills, Geochemistry, Geophysics, Geosystems, 22, https://doi.org/10.1029/2021gc009917, 2021.

Li, J., Mao, J., Min, K.-E., Washenfelder, R. A., Brown, S. S., Kaiser, J., Keutsch, F. N., Volkamer, R., Wolfe, G. M., Hanisco, T. F., Pollack, I. B., Ryerson, T. B., Graus, M., Gilman, J. B., Lerner, B. M., Warneke, C., de Gouw, J. A., Middlebrook, A. M., Liao, J., Welti, A., Henderson, B. H., McNeill, V. F., Hall, S. R., Ullmann, K., Donner, L. J., Paulot, F., and Horowitz, L. W.: Observational constraints on glyoxal production from isoprene oxidation and its contribution to organic aerosol over the Southeast United States, J. Geophys. Res. Atmos., 121, 9849–9861, https://doi.org/10.1002/2016JD025331, 2016JD025331, 2016.

Makar, P. A., Akingunola, A., Aherne, J., Cole, A. S., Aklilu, Y., Zhang, J., Wong, I., Hayden, K., Li, S.-M., Kirk, J., Scott, K., Moran, M. D., Robichaud, A., Cathcart, H., Baratzedah, P., Pabla, B., Cheung, P., Zheng, Q., and Jeffries, D. S.: Estimates of exceedances of critical loads for acidifying deposition in Alberta and Saskatchewan, Atmospheric Chemistry and Physics, 18, 9897–9927, https://doi.org/10.5194/acp-18-9897-2018, 2018.

Meinshausen, M., Vogel, E., Nauels, A., Lorbacher, K., Meinshausen, N., Etheridge, D. M., Fraser, P. J., Montzka, S. A., Rayner, P. J., Trudinger, C. M., Krummel, P. B., Beyerle, U., Canadell, J. G., Daniel, J. S., Enting, I. G., Law, R. M., Lunder, C. R., O'Doherty, S., Prinn, R. G., Reimann, S., Rubino, M., Velders, G. J. M., Vollmer, M. K., Wang, R. H. J., and Weiss, R.: Historical greenhouse gas concentrations for climate modelling (CMIP6), Geoscientific Model Development, 10, 2057–2116, https://doi.org/10.5194/gmd-10-2057-2017, 2017.

Meinshausen, M., Nicholls, Z. R. J., Lewis, J., Gidden, M. J., Vogel, E., Freund, M., Beyerle, U., Gessner, C., Nauels, A., Bauer, N., Canadell, J. G., Daniel, J. S., John, A., Krummel, P. B., Luderer, G., Meinshausen, N., Montzka, S. A., Rayner, P. J., Reimann, S., Smith, S. J., van den

Berg, M., Velders, G. J. M., Vollmer, M. K., and Wang, R. H. J.: The shared socio-economic pathway (SSP) greenhouse gas concentrations and their extensions to 2500, Geoscientific Model Development, 13, 3571–3605, https://doi.org/10.5194/gmd-13-3571-2020, 2020.

Meredith, L. K., Commane, R., Keenan, T. F., Klosterman, S. T., Munger, J. W., Templer, P. H., Tang, J., Wofsy, S. C., and Prinn, R. G.: Ecosystem fluxes of hydrogen in a mid-latitude forest driven by soil microorganisms and plants, Global Change Biology, 23, 906–919, https://doi.org/10.1111/gcb.13463, 2016.

Milkov, A. V.: Molecular hydrogen in surface and subsurface natural gases: Abundance, origins and ideas for deliberate exploration, Earth-Science Reviews, 230, 104 063, https://doi.org/10.1016/j.earscirev.2022.104063, 2022.

Ocko, I. B. and Hamburg, S. P.: Climate consequences of hydrogen emissions, Atmospheric Chemistry and Physics, 22, 9349–9368, https://doi.org/10.5194/acp-22-9349-2022, 2022.

O'Rourke, P., Smith, S., Mott, A., Ahsan, H., Mcduffie, E., Crippa, M., Klimont, Z., Mcdonald, B., Wang, S., Nicholson, M., Hoesly, R., and Feng, L.: CEDS v_2021_04_21 Gridded emissions data, https://doi.org/10.25584/PNNLDATAHUB/1779095, 2021.

Paulot, F., Paynter, D., Naik, V., Malyshev, S., Menzel, R., and Horowitz, L. W.: Global modeling of hydrogen using GFDL-AM4.1: Sensitivity of soil removal and radiative forcing, International Journal of Hydrogen Energy, 46, 13 446–13 460, https://doi.org/10.1016/j.ijhydene.2021.01.088, 2021.

Pétron, G., Crotwell, A., Crotwell, M., Kitzis, D., Madronich, M., Mefford, T., Moglia, E., Mund, J., Neff, D., Thoning, K., and Wolter, S.: Atmospheric Hydrogen Dry Air Mole Fractions from the NOAA GML Carbon Cycle Cooperative Global Air Sampling Network, 2009-Present, https://doi.org/10.15138/WP0W-EZ08, 2023.

Pétron, G., Crotwell, A., Mund, J., Crotwell, M., Mefford, T., Thoning, K., Hall, B., Kitzis, D., Madronich, M., Moglia, E., Neff, D., Wolter, S., Jordan, A., Krummel, P., Langenfeld, R., Patterson, J. D., and Andrews, A.: Atmospheric H_2 observations from the NOAA Global Greenhouse Gas Reference Network, Atmospheric Measurement Techniques, submitted.

Pieterse, G., Krol, M. C., Batenburg, A. M., Steele, L. P., Krummel, P. B., Langenfelds, R. L., and Röckmann, T.: Global modelling of H_2 mixing ratios and isotopic compositions with the TM5 model, Atmospheric Chemistry and Physics, 11, 7001–7026, https://doi.org/10.5194/acp-11-7001-2011, 2011.

Price, H., Jaeglé, L., Rice, A., Quay, P., Novelli, P. C., and Gammon, R.: Global budget of molecular hydrogen and its deuterium content: Constraints from ground station, cruise, and aircraft observations, Journal of Geophysical Research, 112, https://doi.org/10.1029/2006jd008152, 2007.

Prinn, R. G., Weiss, R. F., Arduini, J., Arnold, T., DeWitt, H. L., Fraser, P. J., Ganesan, A. L., Gasore, J., Harth, C. M., Hermansen, O., and et al.: History of chemically and radiatively important atmospheric gases from the Advanced Global Atmospheric Gases Experiment (AGAGE), Earth System Science Data, 10, 985–1018, https://doi.org/10.5194/essd-10-985-2018, 2018.

Prinzhofer, A., Cissé, C. S. T., and Diallo, A. B.: Discovery of a large accumulation of natural hydrogen in Bourakebougou (Mali), International Journal of Hydrogen Energy, 43, 19 315–19 326, https://doi.org/10.1016/j.ijhydene.2018.08.193, 2018.

Rayner, N. A., Parker, D. E., Horton, E. B., Folland, C. K., Alexander, L. V., Rowell, D. P., Kent, E. C., and Kaplan, A.: Global analyses of sea surface temperature, sea ice, and night marine air temperature since the late nineteenth century, J. Geophys. Res. Atmos., 108, 4407, https://doi.org/10.1029/2002JD002670, 2003.

Rodell, M., Houser, P. R., Jambor, U., Gottschalck, J., Mitchell, K., Meng, C.-J., Arsenault, K., Cosgrove, B., Radakovich, J., Bosilovich, M., Entin, J. K., Walker, J. P., Lohmann, D., and Toll, D.: The Global Land Data Assimilation System, Bulletin of the American Meteorological Society, 85, 381–394, https://doi.org/10.1175/bams-85-3-381, 2004.

Röth, E.-P. and Ehhalt, D. H.: A simple formulation of the CH_2O photolysis quantum yields, Atmospheric Chemistry and Physics, 15, 7195–7202, https://doi.org/10.5194/acp-15-7195-2015, 2015.

Sand, M., Skeie, R. B., Sandstad, M., Krishnan, S., Myhre, G., Bryant, H., Derwent, R., Hauglustaine, D., Paulot, F., Prather, M., and Stevenson, D.: A multi-model assessment of the Global Warming Potential of hydrogen, Communications Earth & Environment, 4, https://doi.org/10.1038/s43247-023-00857-8, 2023.

Saunois, M., Stavert, A. R., Poulter, B., Bousquet, P., Canadell, J. G., Jackson, R. B., Raymond, P. A., Dlugokencky, E. J., Houweling, S., Patra, P. K., Ciais, P., Arora, V. K., Bastviken, D., Bergamaschi, P., Blake, D. R., Brailsford, G., Bruhwiler, L., Carlson, K. M., Carrol, M., Castaldi, S., Chandra, N., Crevoisier, C., Crill, P. M., Covey, K., Curry, C. L., Etiope, G., Frankenberg, C., Gedney, N., Hegglin, M. I., Höglund-Isaksson, L., Hugelius, G., Ishizawa, M., Ito, A., Janssens-Maenhout, G., Jensen, K. M., Joos, F., Kleinen, T., Krummel, P. B., Langenfelds, R. L., Laruelle, G. G., Liu, L., Machida, T., Maksyutov, S., McDonald, K. C., McNorton, J., Miller, P. A., Melton, J. R., Morino, I., Müller, J., Murguia-Flores, F., Naik, V., Niwa, Y., Noce, S., O'Doherty, S., Parker, R. J., Peng, C., Peng, S., Peters, G. P., Prigent, C., Prinn, R., Ramonet, M., Regnier, P., Riley, W. J., Rosentreter, J. A., Segers, A., Simpson, I. J., Shi, H., Smith, S. J., Steele, L. P., Thornton, B. F., Tian, H., Tohjima, Y., Tubiello, F. N., Tsuruta, A., Viovy, N., Voulgarakis, A., Weber, T. S., van Weele, M., van der Werf, G. R., Weiss, R. F., Worthy, D., Wunch, D., Yin, Y., Yoshida, Y., Zhang, W., Zhang, Z., Zhao, Y., Zheng, B., Zhu, Q., Zhu, Q., and Zhuang, Q.: The Global Methane Budget 2000–2017, Earth System Science Data, 12, 1561–1623, https://doi.org/10.5194/essd-12-1561-2020, 2020.

Smith-Downey, N. V., Randerson, J. T., and Eiler, J. M.: Temperature and moisture dependence of soil H_2 uptake measured in the laboratory, Geophysical Research Letters, 33, https://doi.org/10.1029/2006gl026749, 2006.

Smith-Downey, N. V., Randerson, J. T., and Eiler, J. M.: Molecular hydrogen uptake by soils in forest, desert, and marsh ecosystems in California, Journal of Geophysical Research, 113, https://doi.org/10.1029/2008jg000701, 2008.

Staffell, I., Scamman, D., Abad, A. V., Balcombe, P., Dodds, P. E., Ekins, P., Shah, N., and Ward, K. R.: The role of hydrogen and fuel cells in the global energy system, Energy & Environmental Science, 12, 463–491, https://doi.org/10.1039/c8ee01157e, 2019.

Taylor, K. E., Williamson, D., and Zwiers, F.: The sea surface temperature and sea-ice concentration boundary conditions for AMIP II simulations, Program for Climate Model Diagnosis and Intercomparison, Lawrence Livermore National Laboratory, University of California, 2000.

van der Werf, G. R., Randerson, J. T., Giglio, L., Collatz, G. J., Kasibhatla, P. S., and Arellano, A. F.: Interannual variability in global biomass burning emissions from 1997 to 2004, Atmospheric Chemistry and Physics, 6, 3423–3441, https://doi.org/10.5194/acp-6-3423-2006, 2006.

van der Werf, G. R., Randerson, J. T., Giglio, L., van Leeuwen, T. T., Chen, Y., Rog̃ers, B. M., Mu, M., van Marle, M. J. E., Morton, D. C., Collatz, G. J., Yokelson, R. J., and K̃asibhatla, P. S.: Global fire emissions estimates during 1997–2016, Earth System Science Data, 9, 697–720, https://doi.org/10.5194/essd-9-697-2017, 2017.

Vollmer, M. K., Walter, S., Mohn, J., Steinbacher, M., Bond, S. W., Röckmann, T., and Reimann, S.: Molecular hydrogen (H_2) combustion emissions and their isotope (D/H) signatures from domestic heaters, diesel vehicle engines, waste incinerator plants, and biomass burning, Atmospheric Chemistry and Physics, 12, 6275–6289, https://doi.org/10.5194/acp-12-6275-2012, 2012.

Wang, H., van Eyk, P. J., Medwell, P. R., Birzer, C. H., Tian, Z. F., Possell, M., and Huang, X.: Air Permeability of the Litter Layer in Broadleaf Forests, Frontiers in Mechanical Engineering, 5, https://doi.org/10.3389/fmech.2019.00053, 2019.

Warwick, N. J., Griffin, N. P., J., K., Archibald, A. T., Pyle, J. A., and Shine, K. P.: Atmospheric implications of increased hydrogen use, Tech. rep., Department of Businnes, Energy & Industrial Stregy Policy Paper, https://www.gov.uk/government/publications/atmospheric-implications-of-increased-hydrogen-use, 2022.

WMO: WMO Greenhouse Gas Bulletin, Tech. Rep. 17, Japan Meterological Agency and WMO, 2021.

Yashiro, H., Sudo, K., Yonemura, S., and Takigawa, M.: The impact of soil uptake on the global distribution of molecular hydrogen: chemical transport model simulation, Atmospheric Chemistry and Physics, 11, 6701–6719, https://doi.org/10.5194/acp-11-6701-2011, 2011.

Zgonnik, V.: The occurrence and geoscience of natural hydrogen: A comprehensive review, Earth-Science Reviews, 203, 103 140, https://doi.org/10.1016/j.earscirev.2020.103140, 2020.